Spring 5-15-2022

Hybrid Double Network Cryogels Scaffold for Repair of Local Cartilage Defect

Kaixiang Zhang
Syracuse University

Abstract

Trauma or repeated injury to the joint can result in focal cartilage defects, which significantly increases the risk of osteoarthritis. Cartilage being avascular has limited self-healing capacity. The current method for treating cartilage defects at early stages involves implantation of autologous chondrocytes with or without a scaffold through invasive surgery; however, invasive surgery can bring pain to patients and post-operative infection risks. Therefore, injectable and biodegradable biomaterials have piqued people's interest. In the current research, we designed a hybrid double network (DN) cryogel by combining multi-arm PEG acrylate and alginate as two networks and crosslinking them at -20°C. Through different characterizations (SEM, mechanical strength, swelling test, etc.), we found that the DN cryogel has a macroporous interconnected structure, high water uptake capacity, and can support chondrocyte growth and extracellular matrix synthesis. These features make it possible for the cryogel to be used as a scaffold for cartilage to treat cartilage defects.

Key words: Cartilage defect, double network cryogels, macroporous interconnection structure

Hybrid Double Network Cryogels Scaffold for

Repair of Local Cartilage Defect

By

Kaixiang Zhang

B.S. Northwest University, 2018

Thesis

Submitted in partial fulfillment of the requirements for the degree of

Master of Science (M.S.) in Chemical engineering

Syracuse University

May 2022

Table of content

List of Figure

List of Table

Chapter 1

Cryogels synthesis and characterization

1. Introduction

1.1. Cartilage

1.1.1. Architecture of cartilage and effect of cartilage defect on joint health

Articular cartilage is a kind of smooth surface that covers the end of the femur and the tip of the tibia. Its function is to help smooth movement of the sliding joint surface, and it can also buffer the end of the bone through weight-bearing.[1] In contrast to most tissues, articular cartilage has no blood vessels, lymphatic vessels, or nerves. It consists of a dense extracellular matrix (ECM) and sparsely distributed chondrocytes. The ECM is mainly composed of water, proteoglycans, and collagen, with lesser amounts of other non-collagen and glycoproteins.[2] Together, these components help retain moisture in the ECM, which is critical for maintaining its mechanical properties. Articular cartilage damage is thought to be the cause of serious musculoskeletal disorders. Articular cartilage is structurally complex and cannot be regenerated, making it challenging to treat and repair cartilage in patients with cartilage defects. Since cartilage has no vascular structure, damaged cartilage has limited ability to heal and repair. Therefore, repairing the normal structure and function of damaged cartilage is one of the most challenging areas in orthopedic research and sports medicine.[3]

Defects in articular cartilage may be due to natural degeneration with age, repeated wear and tear caused by sports, or traumatic events, such as knee abrasions, injuries from jumping from a height, or spraining the knee. Sometimes these injuries are also related to knee fractures or ligament injuries. Occasionally, because there are no nerve endings in the cartilage, these

injuries do not always immediately cause pain. However, patients may experience swelling, stiffness, and mechanical symptoms. Pain may be related to other injuries that occur, such as fractures, bone contusions, ligament injuries, or other severe articular cartilage injuries.[4-5] When a cartilage defect is confined to a specific area within the joint, it is called a focal articular cartilage defect. Focal articular cartilage defects' symptoms include pulsation, pain, swelling, tenderness, and restricted mobility.[6] The degree of articular cartilage damage can range from surface softening to full-thickness bone defects. In addition, the type of damage is also measured by the size of the defect. As the thickness and defect area increase, the size and depth of the defect tend to increase over time. Since cartilage is avascular, it has limited self-healing abilities. In terms of the depth and size of the defect, generally, more severe injuries may require surgery to replace or repair the defect.[7]

1.1.2. Cartilage defect statistic

Defects of focal cartilage injuries are extremely common, and lesions are frequently detected via arthroscopy, even in asymptomatic individuals. Two studies reviewing the incidence of focal cartilage lesions reported the presence of focal lesions in 60-63% of individuals undergoing arthroscopies. The disease burden for the cartilage lesions has tripled from 1996 to 2011 across all gender and age groups. The percentage of patients being treated for cartilage injuries has increased from 13.8 to 22.1%, but less than 1% of these get advanced treatment like chondrocyte transplantation.[8-9]

The high joint injury rates, combined with the inability of the cartilage to heal itself, leaves the patients at high risk of developing osteoarthritis (OA). Osteoarthritis (OA) is currently one of the widespread chronic diseases in the world. Among people 20 years and older, the global incidence of knee OA is 203 per 10,000 people per year.[10] Correspondingly, by 2020,

approximately 86.7 million people 20 years and older worldwide will suffer from knee arthritis each year.[10] The incidence in the United States is 130 cases per 10,000 people per year.[10] The chance of developing OA increases with age (**Figure 1**). OA is generally regarded as a non-serious disease because it does not cause a fatal impact on humans in the short term, but it has a significant impact on patients and their families, and its impact is long-term. The socioeconomic burden of OA is huge. It leads to the development of chronic disability and pain in the affected individual. Thus, early and advanced treatment of joint injuries can prevent or reduce the risk of OA in individuals.
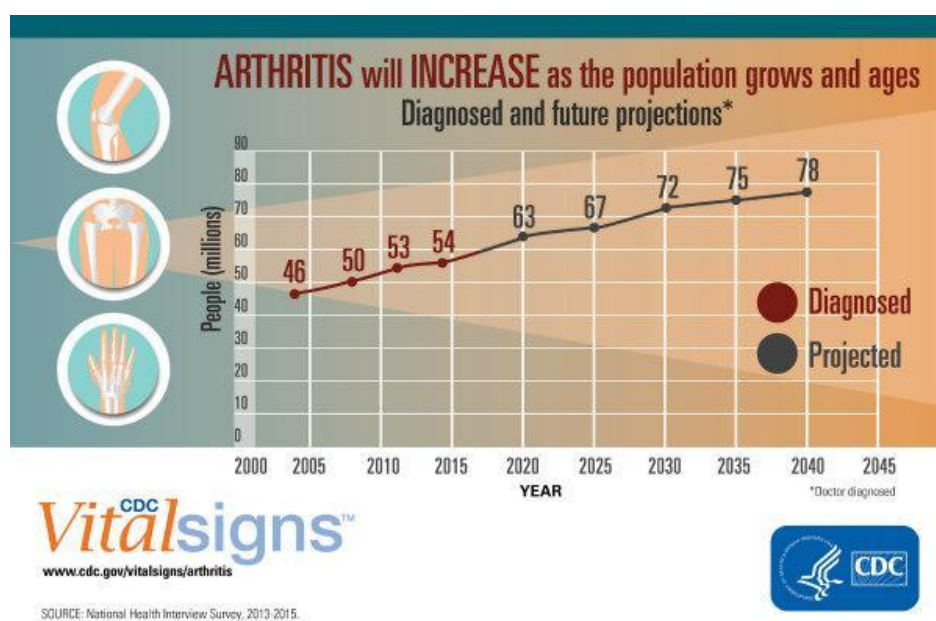
Figure 1. The prevalence of knee osteoarthritis changes with age. Figure is adapted from CDC website.

1.1.3. Traditional treatment for articular cartilage defect

Clinical treatments for localized cartilage defects include arthroscopic debridement, arthroscopic microfracture, Osteochondral Autograft Transplantation (OATS),[11] Autologous Chondrocyte Implantation (ACI)[4], and Osteochondral Allograft. The most common clinical

treatment for focal cartilage defects is arthroscopic chondroplasty or arthroscopic debridement. Arthroscopic debridement, an option to treat cartilage defects, uses a razor to remove loose joint fragments to help smooth the joint defect, thereby improving, but not completely normalizing, the sliding surface. While this procedure provides short-term relief, it makes cartilage more susceptible to wear and tear. Another way to solve cartilage defects is arthroscopic microfracture, making small perforations in the subchondral bone. This allows some blood/bone marrow cells to enter into the defect. This bone marrow enables repair of the defect, thereby forming a new fibrocartilage, which is mostly mechanically inferior compared to original cartilage. In mosaicplasty or osteochondral autograft transplantation (OATs), the core of articular cartilage and bone is removed from another part of the knee joint and transferred to the articular cartilage defect for repair. The OATs procedure results in donor site morbidity, poor integration and degeneration of implanted cartilage over time.[12]

More advanced methods of cartilage regeneration include autologous chondrocyte implantation (ACI), matrix-associated autologous chondrocyte (MACI), and autologous matrix-induced chondrogenesis (AMIC). Both ACI and MACI are two-step procedures in which a piece of articular cartilage is removed through arthroscopy. The piece of cartilage is sent to the laboratory where the cells in the cartilage tissue are separated and cultured to multiply cells to increase the overall number of cells. Later, in ACI, these cells will be re-implanted into the articular cartilage defect of the knee joint. In cases of MACI, the harvested cells from the chondrocyte are expanded in a collagen-based matrix and then re-implanted into the defect site. AMIC, on the other hand, is a single-step procedure that includes implantation of a collagen-based matrix into the defect site in combination with microfracture.[13] These advanced treatments ACI, MACI and AMIC– have shown improved outcomes compared to more traditional treatments. Lastly, osteochondral allograft involves using a piece of cartilage

and bone removed from a cadaveric knee joint. This bone and cartilage are then implanted into the cartilage and bone defect through open surgery in the knee joint.[14] In spite of the high incidence of chondral defects, the number of patients undergoing any type of arthroscopic procedure, traditional or advanced, was only 93/100,000 in 2011.[15] In contrast, patients undergoing total knee arthroplasty (TKA) is fairly high, 429/100,000.[15] Total knee arthroplasty (TKA)[11] remains the most common surgical treatment for arthritis of the knee. The huge disparity between the number of TKA surgeries and articular cartilage repair surgeries indicates an unmet need for better clinical treatments for chondral defects, which can prevent the development of end-stage OA and avoid the need for TKA.[16]

1.2. Tissue engineering strategies to solve cartilage defect

Several cartilage repair methods require surgery and cartilage transplantation. Many of these methods are associated with pain, long postoperative recovery, high morbidity, high cost, and inflammation of the donor sites. Tissue engineering offers a promising alternative strategy by engrafting chondrocytes into biocompatible scaffolds to produce engineered cartilage for repairing damaged cartilage. Tissue engineering can not only help avoid surgery, but also reduce patient suffering and improve clinical outcomes.[17]

1.2.1. Scaffolds for cartilage tissue engineering

Cartilage tissue engineering involves both scaffold-free and scaffold-assisted promotion of neocartilage formation. Scaffold-free techniques mainly rely on generation of cellular aggregates by culturing chondrocytes on non-adherent cultures. These cellular aggregates not only maintain the spherical shape of cells, similar to native cartilage, but also promote cell-to-cell contact and generation of neocartilage with biomechanical and biochemical properties similar to native cartilage. Some of these technologies are in advanced states of clinical trials.

However, in spite of these successes, tissue integration with surrounding cartilage is a challenge yet to be overcome.[18]

Scaffolds play an important role in cartilage tissue engineering. Some of the desired features for a scaffold for cartilage tissue engineering are 1) coordinating scaffold biodegradation and neocartilage growth rate; 2) removal of scaffold byproducts, such as acidic products of degradation; for example, when using poly esters like polyglycolic acid (PGA); 3) biocompatibility of scaffolds; for example, the removal of residual chemicals of scaffold processing, which may be harmful for the cells;[19] 4) incorporating design parameters that allow chondrocytes to maintain spherical morphology similar native chondrocytes;[19-20] 5) mimicking the compressive surface and tensile properties of cartilage. Any mismatch in mechanical properties of implant vs. native cartilage leads to poor integration and shredding of the implanted scaffold due to an imbalance in force distribution. These scaffold-forming materials should also be able to withstand in vivo conditions such as pH and body temperature.[21-22]

Several scaffolds made of natural and synthetic polymers have been tested as matrix systems for culture of chondrocytes and other chondrogenic cells, such as mesenchymal stem cells. Collagen, hyaluronic acid (HA), chitosan (CH), chondroitin sulfate (CS) and other natural materials, such as fibrin, have been shown to be widely used to produce scaffolds for cartilage regeneration. These materials are characterized by biological activity and strong biocompatibility.[23-24] Several scaffolds based on collagen,[25-29] chitosan,[30-31] and hyaluronic acid[32-34] are commercially available and have shown improved clinical outcomes in MACI. However, natural materials are not mechanically stable enough to support cells, so their use as scaffolds produces products that are not sufficient to regenerate tissue.[35-36] Some popularly used synthetic polymers for cartilage tissue engineering are polyesters like poly(lactic-co-glycolic acid) (PLGA),[37-38] polylactic acid (PLA),[39-40] polyglycolic acid (PLG), polyethylene

glycol (PEG),[41-42] polyurethane (PU),[43] and polycaprolactone (PCL).[24, 43-44] Compared with natural materials, synthetic polymers can be used to produce membranes of different shapes by a variety of techniques and, at the same time, can provide better mechanical properties.[35-36] Most of these polymers can be degraded into components that are metabolized in the body after use. Furthermore, by combining these polymers (as copolymers or blends), the mechanical properties and degradation times of the polymers can be controlled.[35-36] However, synthetic materials lack cell adhesion ligands, and degradation products, such as acidic byproducts, can have adverse effects on the site of implantation.[35-36] Recently, there has been great interest in generating hybrid scaffolds combining two different polymers or synthetic and natural polymers. Hybrid scaffolds, combining synthetic and natural polymers allow them to obtain scaffolds of higher mechanical properties than a single network and retain the advantages of natural materials such as cell adhesion sites and biocompatibility, as required for cartilage regeneration.[35-36]

Blends of natural and synthetic polymers have been combined by a variety of methods such as freeze casting, phase separation, porogen leaching and, more recently, 3D printing to generate a variety of scaffolds with an open and interconnected network of pores. Further expanding the use of polymers crosslinked hydrogels have gained a lot of interest for generating appropriate scaffolds for cartilage tissue engineering.[45]

1.2.2. Interpenetrating network of hybrid hydrogels for cartilage tissue engineering

Hydrogels are a crosslinked network of polymers that are highly swollen in aqueous environments whereby 90% of weight is water. Various parameters of hydrogel formation can be tuned. These include crosslinking density, degradation rate, and inclusion of bound or free biochemical factors. Numerous studies have shown promising outcomes when chondrocytes are cultured in 3-D hydrogels.[36, 46] One advantage is the high content of water in hydrogels,

which is similar to native cartilage. An important design parameter for hydrogels to be used for cartilage tissue engineering is mechanical integrity. Traditional single-network hydrogels lack, or are mechanically weak, and thus may not be a suitable scaffold for generating cartilage. Toward advancing the use of hydrogels for cartilage tissue engineering and meeting the requirements of enhanced mechanical strength matching that of native cartilage, hydrogels are being made using multiple polymers.[46-47] Hydrogels made of multiple polymers have far superior mechanical integrity compared to any single network hydrogels that may facilitate better integration with surrounding tissue. In this regard, interpenetrating networks of hydrogels made up of two or more polymer networks have been used for cartilage tissue engineering. For instance, Ingavle et al.[48] incorporated methacrylate chondroitin sulfate as a second network in an agarose-PEG diacrylate hydrogel network. Incorporation of chondroitin sulphate increased the viability of encapsulated chondrocyte and ECM matrix deposition. Another example of a hybrid IPN network is reinforcement of fibrin gels with methacrylated hyaluronic acid (HA). The incorporation of HA increased expression of chondrogenic markers by mesenchymal stem cells.[49]

A special type of interpenetrating networks called double-network (DN) hydrogels have attracted a lot attention due to their exceptional toughness and mechanical strength that can mimic native hyaline cartilage.[50-53] Tough DN hydrogels consist first of a network forming a rigid structure while a second network is soft and ductile. A DN is synthesized by a two-step sequential radical polymerization of the two polymer networks.[54] Typical polymers used for DN hydrogels consist of a combination acrylamide polyelectrolytes poly(2-acrylamido-2-methylpropanesulfonic acid) (PAMPs) or poly(N,N-dimethylacrylamide) with neutral acrylamide polymers like polyacrylamide.[51, 55] More recently, natural polymer like hyaluronic acid and gelatin has been combined to generate double network hydrogels for cartilage tissue engineering.[56] During polymerization, the rigid and brittle polymer network forms a tightly

cross-linked network structure with a high overall cross-linker concentration. This brittle polyelectrolyte hydrogel is fully swollen in a high-concentration neutral monomer aqueous solution containing a lower concentration of a cross-linking agent, and then the second monomer polymerizes with the network structure to form a flexible network inside the first network hydrogel.[54] Recent in vivo studies using DN hydrogels for cartilage regeneration show increase in sulphated glycsoaminoglycans (GAGs) and type 2 collagen, the typical components of native, healthy cartilage.[56-58] However, owing to a very high crosslinking density and non-degradability of the DN hydrogels, no cell infiltration is observed. Polymers used for DN hydrogels are often non-degradable, which renders DN hydrogels impermeable to cells and, in the long-term, limit deposition of ECM.[47]

A variation of DN hydrogels, which has been developed recently, is a hybrid gel consisting of a covalently crosslinked network interpenetrating with an ionically linked network of natural polymers. The combination of these two networks as IPN results in a highly tough, stretchable and self-healing hybrid hydrogels. The replacement of one of the covalent networks with non-covalent ionically crosslinked network allows for recoverable energy dissipation and self-healing of the gel after a certain delay. Unlike DNs with two covalent networks, these hybrid gels retain fracture toughness on repeated loading.[59] A hybrid interpenetrating network of PEG diacrylate and sodium alginate crosslinked via free radical crosslinking and ionic crosslinking, respectively. The hybrid IPN exhibited high fracture toughness and stretchability, which exceeded natural cartilage. The hydrogels maintained high cell viability and promoted the expression of ECM.[60] Some other polymers that have been used to form the non-covalent network in these hybrid double network gels include polyvinyl alcohol, chitosan, and agar etc while the covalent network is exclusively formed via free-radical crosslinking of acrylamide or PEG diacrylate.[61-63] However, the use of a covalent network formed via free radical crosslinking makes these hybrid DN gels non-degradable. Moreover, with the exception of a

few examples, most hybrid DN gels are non-porous in nature. These limit the application of hybrid DN gels for cartilage tissue engineering. Several studies have shown that porous structure and degradability are important for cell infiltration and ECM matrix deposition for cartilage constructs.[64-65]

In this study, we aim to overcome the limitation of current hybrid DN gels by generating ice-template, hybrid macroporous double network cryogels of PEG and alginate using biocompatible click chemistry for covalent network formation and ionic non-covalent bonding in alginate networks.

1.2.3. Definition of cryogels

Cryogels are macroporous hydrogels, which are made at sub-zero temperatures. The process of generating cryogels is essentially different than the typical freeze-drying process for generating macroporous hydrogels. To make cryogels, gel precursors along with crosslinkers are mixed and then frozen at sub-zero temperatures (typically -5°C to -20°C). The gel precursors undergo chemical or physical crosslinking in a frozen state. [66-67] The main stage of cryogel synthesis is in the freezing state, during which chemical reactions take place leading to gelation. During the freezing process, most of the solvents crystallize by freezing. These solvent crystals can act as porogens, while the hydrogel components remain in the liquid microphase around them. A cryogel with an open, interconnected macroporous structure is formed upon the thawing and melting away of the ice crystals.[68-71]

The freezing rate significantly affects the pore size and porosity of cryogels. Slower freezing rates may result in larger pores and increased structural interconnectivity. In contrast, faster freezing rates produce cryogels with weaker mechanical strength and lower levels of pore interconnection. This may be because at very low temperatures the ice nuclei generated

are very small and do not grow enough to generate interconnected pore networks.[72-76] Furthermore, the resulting network is spongy, mechanically stable, and can be compressed to at least half its length without damage.[77-79] After hydration, cryogel pores become rounded due to the liquid and surface tension of the pore walls. In addition, the macroporous structure facilitates rapid swelling and homogenous cellular infiltration. The physical properties of cryogels, especially pore size, can be influenced by adjusting parameters such as polymer content and concentration, crosslinker mechanism and concentration, freezing time, temperature and freezing/thawing cycles.[69, 80-85] To confirm that cryogels have the appropriate properties for application to a particle tissue, typical characterization of cryogels includes analysis of pore size and overall degree of interconnectivity. Mechanical durability is also assessed by a combination of compression and tensile tests.

1.2.4. Cryogels for cartilage tissue engineering

DN (double network) cryogels and SN (single network) cryogels: Single network cryogels are gels synthesized from only one polymer at sub-zero temperature. Compared with single-network cryogels, interpenetrating network[69, 81-83, 85-86] and double-network cryogels are gels synthesized from two kinds of polymers at sub-zero temperature.[87-90] DN cryogels usually tend to have stronger mechanical strength.[91-92]

In this study, we designed hybrid double network cryogels with interconnected macroporous structures that provide a favorable environment for chondrocyte adhesion, proliferation, and matrix formation. We first synthesized hybrid double network and single network cryogel scaffolds based on multi-arm PEG acrylate with and without alginate and then performed a series of characterizations to assess the internal structure, mechanical strength, water uptake capacity and degradation of cryogels. Finally, we assessed the suitability of the cryogels for culturing mouse-knee derived chondrocytes in the cryogels. Our results indicate

the hybrid double network cryogels with macroporous interconnected structure can provide a suitable scaffold for culture of primary chondrocytes.

2. Materials and methods

2.1. Overview

We first synthesized hybrid DN (double network) cryogels, using sodium alginate as one of the networks with multi-arm PEG acrylate (4 arm PEG acrylate (MW:10kDa) or 8 arm PEG acrylate (MW: 10kDa)) as the second network. The multi-arm PEG acrylate network was crosslinked via a dithiol crosslinker (Dithiothreitol (DTT), Dithiobutylamine (DTBA) or PEG dithiol.) using Michael addition chemistry between thiol and acrylate. A combination of different dithiol crosslinker and multi-arm PEG acrylate generated a crosslinked network with different density of thioester bonds, which led to different degradation rates of the network. The hybrid DN cryogels were characterized for pore structure, mechanical properties, the degradation rate, and the equilibrium swelling rate. Finally, chondrocytes were seeded onto the hybrid DN cryogels and analyzed for sulfated glycosaminoglycan (sGAG) synthesis.

2.2. Hybrid DN cryogels synthesis

Alginate-PEG DN cryogels were synthesized by combining multi-arm PEG acrylates with di-thiol crosslinkers, while alginate was combined with calcium salt and were frozen for a specified length of time. First 20 % w/v solution of multi-arm PEG was mixed with 1% w/v alginate solution made in 0.01 M HEPES buffer of pH 7.2. Next, the calcium carbonate (0.03M) and glucono-delta-lactone (GDL) (0.06M) (molar ratio of $CaCO_3$: GDL is 1:2) was added to the mix to initiate the crosslinking of the alginate network. Finally, a dithiol crosslinker (DTT, DTBA or PEG dithiol) was added to the mix in a 1:1 molar ratio of acrylate:

thiol. All preparation of gel precursor solutions was done over ice to maintain low temperatures and to prevent any premature gelation before the precursor solution was frozen. Once all crosslinkers were added, the solution was quickly transferred into a plastic vial. The vial was sealed and placed in a cryostat set at -20°C and maintained in a frozen state for 18 hours to allow for complete gelation (**Figure 2**). After incubation the cryogels were thawed at room temperature and washed with water to remove any unreacted precursors. The macroporous cryogels obtained are freeze dried for further use. The different precursors used for DN cryogel preparation and their concentration are listed in **Table 1 and Table 2** below.
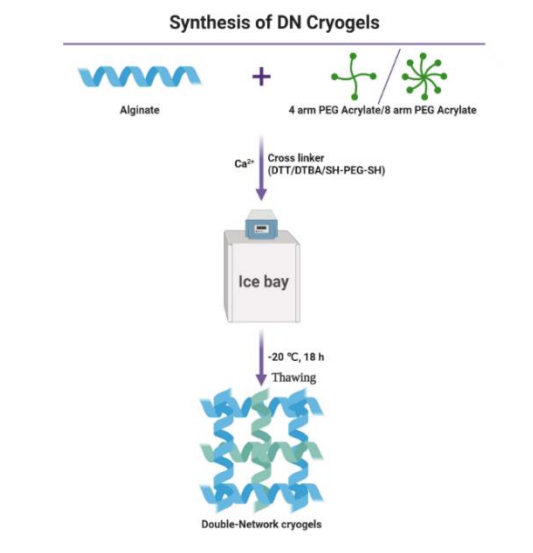
Figure 2. Synthesis of Alginate- PEG hybrid DN (double network) cryogels.

Table 1. Structure and properties of multi arm PEG Acrylate.
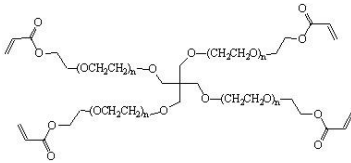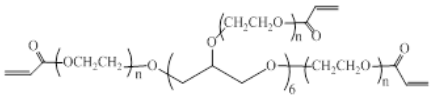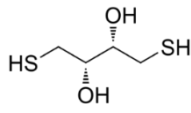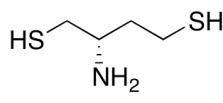
Network	Abbreviation	MW (Da)	Structure
4 arm PEG acrylate	4-arm PEGAc	10k	
8 arm PEG acrylate	8-arm PEGAc	10k	

Table 2. Structure and properties of dithiol crosslinkers used for the synthesis of PEG network in hybrid DN cryogels.

Crosslinker	Abbreviation	MW (Da)	Structure
PEG dithiol	PEG-diSH	3400	SH——$(CH_2CH_2O)n\,CH_2CH_2$——SH
Dithiolerthritol	DTT	154	
(S)-2 Aminobutane 1,4 dithiol	DTBA	177	

2.3. Characterization of DN cryogels

2.3.1. Scanning Electron Microscopy

Scanning electron microscopy (SEM) analysis was performed on different double network cryogels and single network cryogels. All samples were dried in ethanol gradient.[93] The

samples were cut into 5 mm height discs and placed into ethanol with increasing concentrations(20 %, 40 %, 60%, 80 % v/v) for 5 minutes each. Finally, the samples were placed in 100% (v/v) ethanol for 30 minutes for complete dehydration. The samples were then vacuum dried overnight using a lyophilizer before gold plating. Dried and gold coated cryogels were imaged using JEOL JSM 5600 SEM.

2.3.2. Fourier-transform infrared spectroscopy

Fourier-transform infrared spectroscopy (FTIR) analysis was performed on different double network cryogels and single network cryogels. All samples were dried in a gradient of ethanol as described for SEM microscopy. The dried cryogels were placed in an FTIR instrument (Thermo IS5) for testing, to obtain an infrared spectrum. Each spectrum was recorded in the range of 500 to 4000 cm^{-1} at a resolution of 4 cm^{-1} and 64 scans per spectra. The chemical composition of cryogels was inferred by the relative positioning of the peaks in the FTIR spectrum.

2.3.3. Mechanical strength

Universal compression and tensile tester was used to perform tensile and compression tests on DN cryogels and SN cryogels (**Figure 3**). In the tensile test, a sample with a diameter of 12 mm and a length of 2.5 mm was placed between two clamps, and the cryogels were stretched at a speed of 2 mm/sec until the sample was broken. The tensile force was recorded, and the change in sample length caused by the stretching was measured.

In the compression test, a sample with a diameter of 12 mm and a length of 5 mm was placed between the two plates of the load frame. The sample was then compressed at a speed of 2 mm/sec to 70% of the total length. The compression force was recorded, and the column

length change caused by the compressing was measured. The following equations were used to estimate the tensile modulus and compression modulus of the whole cryogels:

Strain =ΔL/L   Stress=F/A   E=(F/A)/(ΔL/L)

Where E is the Young's modulus of elasticity, F is the applied force, A is the cross-sectional area of the sample, L is the initial length of the sample, and Δ L is the change in length under tensile and compressive forces. The linear region of the stress vs strain graphs was analyzed to obtain the elastic modulus for each sample. Three replicates per cryogel were analyzed, and the elastic modulus values were expressed average ± SD.
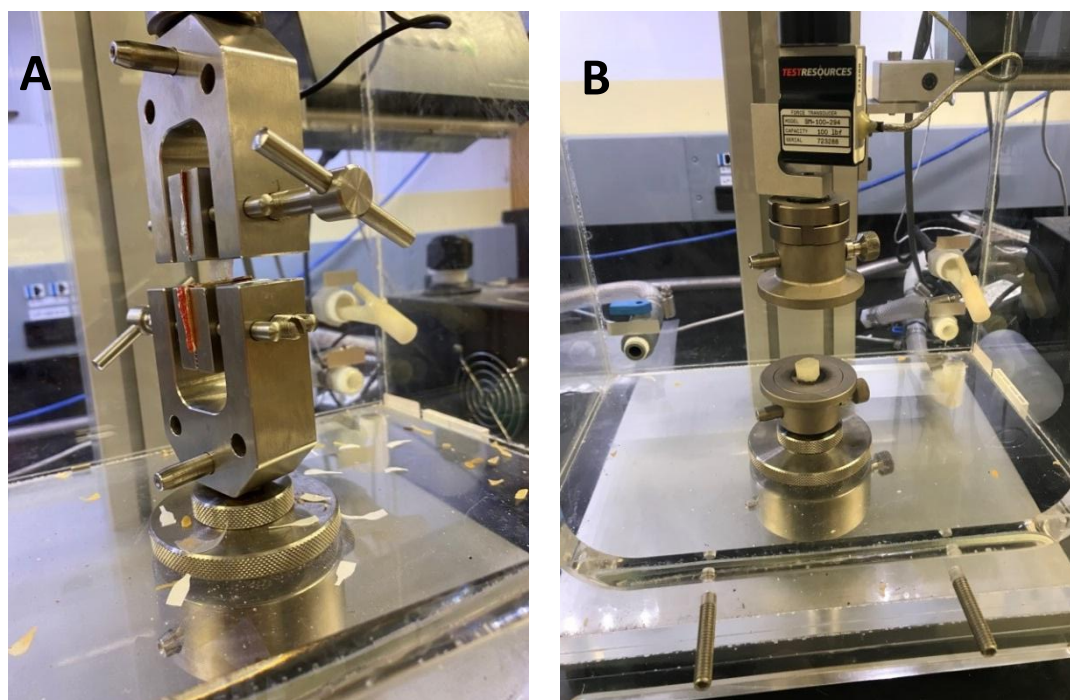
Figure 3. Mechanical strength test on double network cryogels. **A)** tensile test (left image) **B)** compression test (right image).

2.3.4. Swelling kinetics and degradation test

The swelling kinetics were measured using a conventional gravimetric method.[2] Briefly, each cryogel sample was cut to a length of 2.5 mm with a diameter of 12 mm and dried. Dried

cryogels samples were placed in phosphate buffer saline (PBS) (with 2 mM $CaCl_2$) and maintained at room temperature (RT). The water absorption rate was measured by weighing the samples at regular time intervals and calculating the change in weight over time. The cryogels were removed from the swelling medium at 2 min, 5 min, 30 min, 1 h, and 1 day. The excess water on the surface was wiped off by the filter paper. After regular intervals, the weight of the gels was taken until equilibrium was reached. Three replicates of similar size, per cryogel, were used for the study. The water uptake capacity of the cryogels was determined using the formula:

Water uptake capacity (Wu) (%) formula:

Wu = [(Mt-Mg)/(Mg)] *100

Wu is water uptake capacity, Mt is weight of cryogels at a given time interval, Mg is weight of air dried cryogels.

The degradation rate of the cryogels was measured in a similar manner as the swelling kinetics. Briefly, it involved measuring the change in dry weight of the cryogel at regular intervals after maintaining them in PBS at 20 °C. Different hybrid DN cryogels and SN cryogels were vacuum dried overnight with a lyophilizer, and then kept in a vacuum dryer until further use. The dried cryogels were swelled in PBS either containing 2 mM $CaCl_2$ or 10 mM EDTA to chelate calcium. Each cryogel sample had a length of 2.5 mm and a diameter of 12 mm. Hydrogel samples of similar compositions made at room temperature were used as control.

Degradation (%) formula:

Degradation (%) = (Mt-Mi)/(Mi*100)

Mt is the weight of cryogels at a given time interval, Mi is initial weight of cryogels.

2.3.5. Rheometer test

All rheology experiments were performed using a temperature-controlled lower peltier plate geometry rheometer (TA instruments DHR3). For rheological testing, 8-arm PEG acrylate-DTBA with alginate DN cryogels, 8-arm PEG acrylate-PEG dithiol add alginate DN cryogels and 8-arm PEG acrylate-PEG dithiol SN cryogels were fabricated into 12 mm diameter and 5 mm thick disks. The disks were equilibrated in $1\times$ PBS, pH 7.4 for 2 hours at 37 °C. Excess water from the surface of the cryogel was wiped off using KimWipe® prior to measurement. All cryogels were tested at a frequency of 1 rad s^{-1} and a constant strain of 1% (in the linear viscoelastic region).

2.3.6. Chondrocyte isolation and seeding on cryogels

Freshly sacrificed mice (n =20) were obtained from the Syracuse University animal facility. Mice knees were isolated, and the knee articular cartilage was harvested and then washed with PBS. The cartilage was then placed in 3 mg ml $^{-1}$ collagenase D solution for digestion, [36], for 45 minutes (**Figure 4**). The collagenase solution was then diluted to 0.5 mg ml $^{-1}$ with the cartilage still in the solution. The solution was incubated overnight, in an incubator maintained at 37 °C and 5% CO_2. The cartilage disintegrated into smaller aggregates and individual cells. The next day, the digestive solution with residual cartilage was taken out and placed in a tube, then centrifuged to obtain a cell pellet of chondrocytes. The chondrocytes were resuspended in the Dulbecco's modified eagle medium (DMEM) complete cell culture medium with 10% fetal bovine serum (FBS) and 1% penicillin streptomycin (PS) with L-glutamine. The chondrocytes cells were plated in a tissue culture treated polystyrene (TCPS) petri dish and cultured in an incubator maintained at 37 °C and 5% CO_2 until used.

Freshly prepared cryogels were sterilized with 70% ethanol, cut into 4 equal parts inside a biosafety cabinet. After the evaporation of ethanol completely dried the cryogels, they were placed in a well of a 48 well plate. Previously isolated and cultured mouse chondrocytes were resuspended following detachment using trypsin. The chondrocytes were resuspended in complete medium and 300 µL of chondrocyte suspension was added to each cryogel sample with 200000 cells/gel. Chondrocytes seeded onto well plates directly were used as positive control. The chondrocytes were maintained for 10 days and then used for further quantification of sGAG secretion by chondrocytes.

2.3.7. Measurement of sGAG secretion

After culturing for about ten days, the cryogels were removed from the culture medium and collected. The cryogels were chopped into smaller pieces and incubated in a papain digestion buffer and a alginate lyase. The samples were placed in a heating block maintained at 60-65°C for at least 4 hours to completely dissolve the cryogels. The digested samples were stored at -80 °C and were subsequently used for sGAG measurement.

The sGAG concentration in cryogel samples was measured using dimethylmethylene blue (DMMB) assay. A DMMB stock with 2 different concentrations 34 mg/ml and 16 mg/ml was prepared in 100% ethanol. The stocks were then diluted in a buffer and the pH was adjusted to 1.5. The DMMB dyes solution made from two different stock concentrations were mixed at fixed ratios and a baseline OD at 525 nm is adjusted to fall between $0.3 < OD_{525} < 0.34$. Next, chondroitin sulfate standards were prepared in the papain digest buffer. Twenty microliters of samples and standards are placed in 96 well plates and mixed with 300 µl of the DMMB dye. The colorimetric change was immediately recorded at 525 nm using a plate reader. The OD of samples was compared to the chondroitin sulfate standards to determine the concentration of sGAG formed in each cryogel sample.
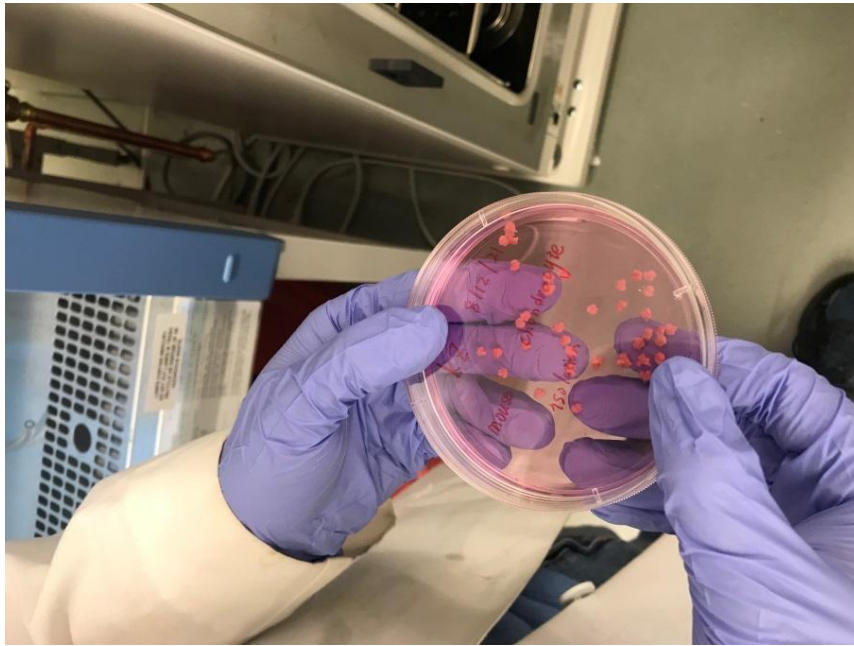
Figure 4. Cartilage harvested from mice knee incubated in collagenase solution for digestion.

3. Results

3.1. Synthesis of cryogels

In this study, we first optimized different parameters for cryogel synthesis. Some of the different parameters that we studied are listed in **Table 3.**

Table 3. Different synthesis parameters for cryogels that were evaluated in this study.

Cryogel Components		Additivies	Temperature	Cryogel properties	
Network 1 - Alginate	Network 2 - multi-arm PEG acrylate			Porosity	Qualitative mechanical properties
1% w/v Alginate + 1 mM CaCl$_2$	10 % w/v 4-armPEG acrylate		Freezer (-20 C)	no pores	Most are liquid and cannot form gels
1% w/v Alginate + 2 mM CaCl$_2$	10 % w/v 4-armPEG acrylate		Freezer (-20 C)	no pores	Most are liquid and cannot form gels
1% w/v Alginate + 1 mM CaCl$_2$	20 % w/v 4-armPEG acrylate		Freezer (-20 C)	no pores	Most are liquid and cannot form gels
1% w/v Alginate + 1 mM CaCl$_2$	30 % w/v 4-armPEG acrylate		Freezer (-20 C)	no pores	Most are liquid and cannot form gels
1% w/v Alginate + 1 mM CaCl$_2$	20 % w/v 4-armPEG acrylate (10 kDa)+ DTT		Cryostat (-12 C)	moderate porosity	Can form gels, poor mechanical integrity
1.5% w/v Alginate + 1mM CaCl$_2$	10 % w/v 4-armPEG acrylate (10 kDa)+ DTT		Cryostat (-12 C)	no pores	Can form gels, poor mechanical integrity
1% w/v Alginate + 1mM CaCl$_3$	10 % w/v 4-armPEG acrylate (10 kDa)+ DTT	freeze and thawing	Cryostat (-12 C)	moderate porosity	Can form gels, poor mechanical integrity
1% w/v Alginate + 6mM CaCO$_3$+12mM GDL	10 % w/v 4-armPEG acrylate (10 kDa)+ DTT		Cryostat (-12 C)	moderate porosity	Can form gels, poor mechanical integrity
1% w/v Alginate + 6mM CaCO$_3$+12mM GDL	10 % w/v 4-armPEG acrylate (10 kDa)+		Cryostat (-12 C)	moderate porosity	Can form gels, but has poorest mechanical properties
1% w/v Alginate + 6mM CaCO$_3$+12mM GDL	10 % w/v 4-armPEG acrylate (10 kDa)+ 4 arm-PEG-SH		Cryostat (-12 C)	moderate porosity	Can form gels, poor mechanical integrity
1% w/v Alginate + 6mM CaCO$_3$+12mM GDL	10 % w/v 4-armPEG acrylate (10 kDa)+ DTT	0.1% DMSO	Cryostat (-12 C)	moderate porosity	Can form gels, poor mechanical integrity
1% w/v Alginate + 6mM CaCO$_3$+12mM GDL	10 % w/v 4-armPEG acrylate (10 kDa)+ DTT	1% DMSO	Cryostat (-12 C)	moderate porosity	Can form gels, poor mechanical integrity
1% w/v Alginate + 6mM CaCO$_3$+12mM GDL	10 % w/v 4-armPEG acrylate (10 kDa)+ DTT	10% DMSO	Cryostat (-12 C)	moderate porosity	Can form gels, poor mechanical integrity
1% w/v Alginate + 6mM CaCO$_3$+12mM GDL	10 % w/v 4-armPEG acrylate (10 kDa)+ DTT	1% kaolinite	Cryostat (-12 C)	moderate porosity	Can form gels, poor mechanical integrity
1% w/v Alginate + 6mM CaCO$_3$+12mM GDL	10 % w/v 4-armPEG acrylate (10 kDa)+ DTT	10% DMSO and 1% kaolinite	Cryostat (-12 C)	moderate porosity	Can form gels, poor mechanical integrity
1% w/v Alginate + 6mM CaCO$_3$+12mM GDL	10 % w/v 8-armPEG acrylate (10 kDa)+ DTT		Cryostat (-12 C)	moderate porosity	Can form gels, poor mechanical integrity
1% w/v Alginate + 6mM CaCO$_3$+12mM GDL	20 % w/v 8-armPEG acrylate (10 kDa)+ DTT		Cryostat (-12 C)	no pores	Mostly liquid and cannot form gels
1% w/v Alginate + 6mM CaCO$_3$+12mM GDL	20 % w/v 8-armPEG acrylate (10 kDa)+ DTT		Cryostat (-20 C)	moderate porosity	Can form gels, poor mechanical integrity
1% w/v Alginate + 6mM CaCO$_3$+12mM GDL	20 % w/v 8-armPEG acrylate (10 kDa)+ DTT		Cryostat (-20 C)	interconnect macroporous	Yellow, elastic, good mechanical integrity
1% w/v Alginate + 6mM CaCO$_3$+12mM GDL	20 % w/v 8-armPEG acrylate (10 kDa)+ PEG dithiol		Cryostat (-20 C)	interconnect macroporous	Pink, small size, moderate mechanical integrity
1% w/v Alginate + 6mM CaCO$_3$+12mM GDL	20 % w/v 8-armPEG acrylate (10 kDa)+ DTBA		Cryostat (-20 C)	interconnected macropores	Yellow, larger in size, slightly brittle compared to add DTT
1% w/v Alginate + 6mM CaCO$_3$+12mM GDL	20 % w/v 4-armPEG acrylate (10 kDa)+ DTT		Cryostat (-20 C)	moderate porosity	White, elastic, good mechanical integrity

The first parameter we studied was the synthesis temperature of DN cryogels. Temperature is a critical parameter for synthesis of cryogels. Cryogels are made at sub-zero temperature as described in the introduction. The lower the freezing temperature, the smaller the ice crystals are, and smaller the pore size. Besides, the rate of reaction is also influenced by the temperature chosen for cryogel formation. Below certain temperatures, the rate of reaction becomes impractically slow, leading to no crosslink/gel formation.[78, 82, 94] Thus, based on these limits we choose three different synthesis temperatures -8°C, -12°C, and -20°C for synthesis of cryogel. Qualitatively, comparing the physical appearance (opaque vs translucent) and mechanical integrity, based on touch of DN cryogel synthesized at different temperatures, showed that   -20°C is the optimum temperature for cryogel synthesis.

Next, we optimized the concentration of two networks and the crosslinking agent concentration. The first network we tried was 1% or 1.5% w/v alginate. When alginate solution concentration exceeds 1.5%, the alginate solution becomes excessively viscous and cannot be used to synthesize cryogels. Thus, we used only 1% w/v alginate for cryogels. In the case of the alginate network, we initially used $CaCl_2$ as the crosslinker initiator. However, due to the very fast kinetics of reaction it was difficult to control gelation of alginate before freezing. Thus, we switched to $CaCO_3$ and gluconolactone (GDL) as the crosslinker initiator for the alginate network. The $CaCO_3$ and GDL pair allows slow gelation (15 to 30 min depending on molar concentration) of the alginate network. The slower kinetics allowed us enough time to work with our solution before freezing them for gelation.

For the second network, we used 10% and 20% w/v 4-arm PEG acrylate (10 kDa) and 8-arm PEG acrylate (20 kDa). It was found that when using 4-arm PEG acrylate as the second network to synthesize DN cryogels with 1% alginate, a 20% w/v concentration of multi-arm

PEG acrylate was most optimal for synthesis. However, we observed that DN cryogels synthesized using 4-arm PEG acrylate (10 kDa) and 8-arm PEG acrylate (20 kDa).

Further, to obtain the interconnected macroporous structure, we added different additives which interfere with ice crystal formation. One of the challenges that we faced in generating cryogels using the Michael addition reaction for the PEG network formation, was the lack of a macroporous structure. We postulated that this may be due to high concentrations of both alginate and PEG. Both PEG and alginate are known to interfere with the formation of ice crystals, thus their combined presence depresses the temperature for ice crystal formation and further inhibits ice formation at -20 °C, leading to a non-porous network. Thus, to induce formation or to manipulate ice formation, we tried 2 different additives: dimethyl sulfoxide (DMSO) and kaolinite. Kaolinite's surface is known to promote ice nuclei formation and thus can help in ice nuclei formation in our system.[95] DMSO is a cryoprotectant solvent but also freezes at a much higher temperature.[96] Thus, it may help in ice crystal formation at a much lower temperature. However, we saw only a modest increase in porosity of these gels post addition of either DMSO or kaolinite. Only when both DMSO and kaolinite were combined did we obtain optimal porosity.

Last, we made cryogels using 8-arm PEG acrylate (10 kDa) instead of 20 kDa MW. The hybrid DN cryogels, made using 8-arm PEG acrylate, as one of the networks resulted in the formation of macroporous structures, as can be seen in the SEM images. The macroporous interconnected structure was not obtained when using 4-arm PEG acrylate (10 kDa) and 8-arm PEG acrylate (20 kDa) as one of the networks (**Figure 5**). We believe that the MW of the PEG precursor played a critical role in ice crystal formation. Use of the small molecular weight PEG precursor, did not inhibit ice formation as much and thus we were able to obtain a macroporous structure. At this stage we also tested multiple multi-arm thiol crosslinkers (4-arm: 4-arm PEG-

SH, 3-arm: pentaerythritol; and dithiol crosslinkers: DTT, DTBA and PEG dithiol). We chose a 4-arm crosslinker to react with a 4-arm PEG acrylate, as studies have shown the formation of more homogenous and tougher networks if the 4-arm crosslinker is combined with the 4-arm PEG acrylate.[97] However, we had limited success in obtaining cryogels with 4-arm or 3-arm thiol crosslinkers. Finally, we tested a series of dithiol crosslinkers as listed in **Table 1**. These crosslinkers resulted in the formation of cryogels of varying strength and were optimized for further use. To conclude, in this study, we found that the optimal composition of hybrid DN cryogels was 1% w/v alginate crosslinked with $CaCO_3$ and GDL + 20% w/v 8-arm PEG acrylate (10 kDa) crosslinked with dithiol crosslinkers.
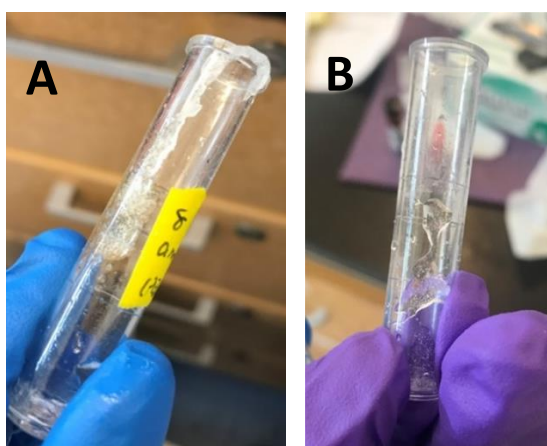
Figure 5. Images of cryogels which did not result in a macroporous structure with adequate mechanical integrity: A) the shape of cryogels is irregular with no mechanical integrity, B) or the crosslinking reaction was not efficient, and gel is a liquid after incubation under frozen conditions.

3.2. SEM analysis of macroporous structure of cryogels

SEM image shows the pore structure of cryogels in **Figure 6.** We found that the DN cryogels prepared with 8-arm PEG acrylate have a macroporous interconnected structure (Figure 10 A&B) with a pore size range of 10-50 μm. Contrary to this the DN cryogels prepared

with 4-arm PEG acrylate do not show a macroporous structure (**Figure 6 D**). The structure of 8 arm PEG SN cryogels is porous (**Figure 6 E&F**), but does not seem to have pore interconnectivity. The macroporous structure in cryogel is formed as a result of the polymerization of gel precursors around the frozen ice crystals. Upon thawing, these crystals melt away, leaving behind an ice-templated macroporous interconnected network. The difference in pore structure between DN cryogels of 4-arm acrylate and 8-arm PEG acrylate could be attributed to the MW of the individual arm. As discussed above, PEG inhibits ice formation.[98] The efficiency of cryoprotection action of PEG is dependent on the molecular weight of PEG. Thus, when we used 4-arm PEG acrylate vs 8-arm acrylate 10 kDa, the individual MW of each arm changed from 2.5 kDa to 1.25 kDa. We believe that this change in MW of the PEG precursor played a critical role in facilitating ice crystal formation and thus the interconnected pore network in DN cryogels. Use of the small molecular weight PEG precursor did not inhibit ice formation as much and thus we were able to obtain macroporous structure.[99-101] Thus**,** 8-arm PEG acrylate is more suitable for the network for preparing DN cryogels. Lastly, use of different dithiol crosslinkers did not affect the pore architecture,[102] and similar pore size and morphology was observed for both DTT and PEG-dithiol crosslinker in 8-arm PEG acrylate+ alginate DN cryogel irrespective of the crosslinker MW.
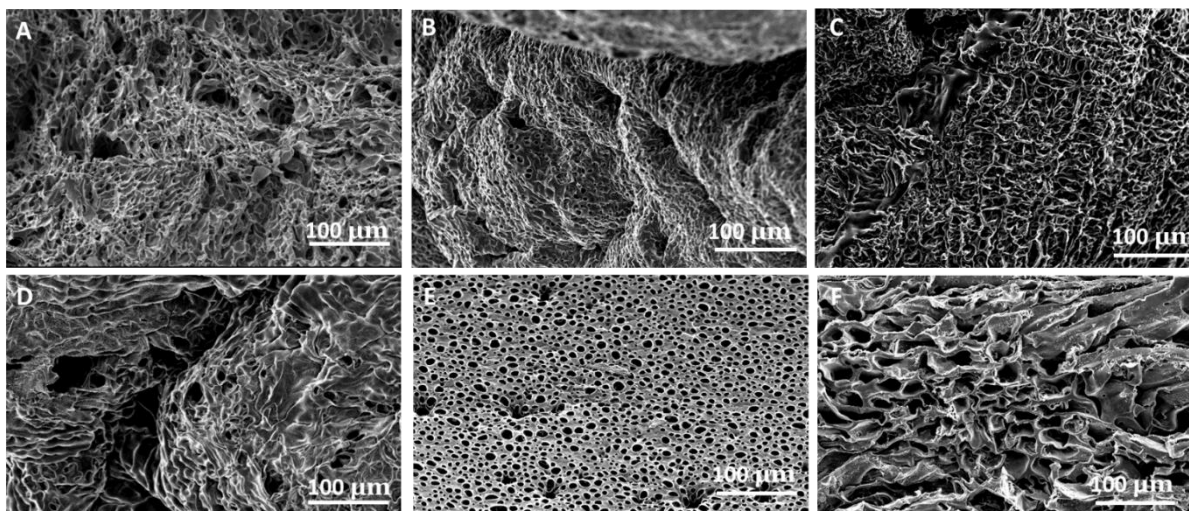
Figure 6. SEM images of DN and SN cryogels. A) 8-arm PEG acrylate-DTT+ alginate DN cryogels; B) 8-arm PEG acrylate-PEG dithiol + alginate DN cryogels; C) 8-arm PEG acrylate-DTBA+ alginate DN cryogels D) 4-arm PEG acrylate-DTT+ alginate DN cryogels; E) 8-arm PEG acrylate-DTT SN cryogels; F) 8-arm PEG acrylate-DTBA SN cryogels.

3.3. FTIR analysis of cryogels

FTIR images of the DN cryogels and SN cryogels is shown in **Figure 7 A & B**. Comparing the FTIR diagrams of DN cryogels, I found 8 arm PEG acrylate-PEG dithiol with alginate DN cryogels and 8 arm PEG-DTT with alginate DN cryogels have a peak at 3330 cm^{-1} and 1610 cm^{-1}. The peak at 3300 - 3400 cm^{-1} is a result of -OH stretching in alginate while the 1610 peak is a result of stretching vibrations of the carboxylate anions.[103] The peak corresponding to C=O is seen at 1732 cm^{-1} in both SN and DN cryogels, showing that both PEG and alginate have incorporated in the DN network. In SN PEG cryogels the peak corresponding to C=C at 1610 cm-1 is not seen owing to a formation addition reaction between C=C of 4-arm PEGAc and SH of the dithiol crosslinker. The peak at 1610 cm-1 reappears in the DN because of the presence of the -COOH in alginate. These peaks prove that the DN cryogel has carbonyl and hydroxyl groups, which are present in the alginate

chain and the PEG acrylate reaction with thiol forms the second network. By FTIR spectra we demonstrated that DN cryogels contain alginate but SN cryogels do not.
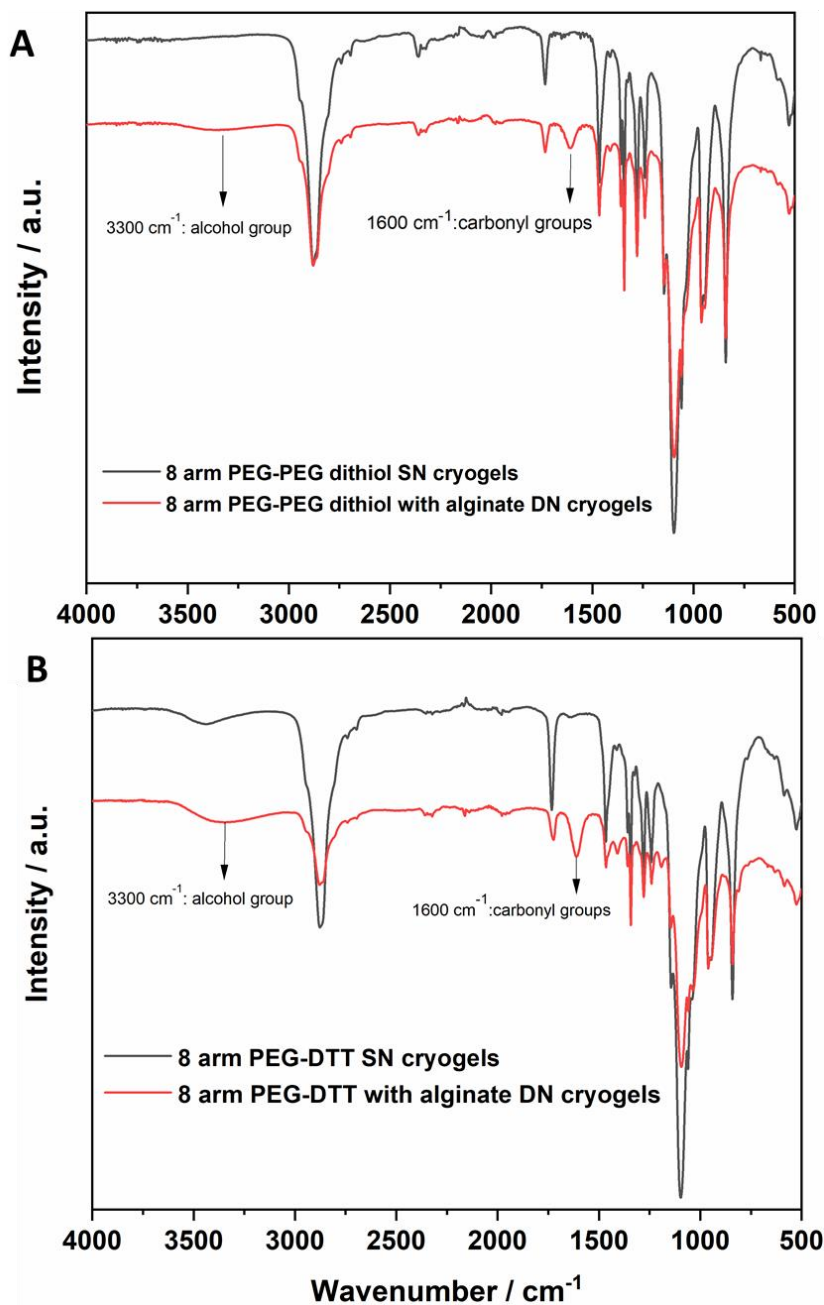
Figure 7. Comparing ATR-FTIR spectra of DN and SN cryogels of PEGacrylate-dithiol and alginate. A) 8-arm PEG acrylate-PEG dithiol with alginate DN and 8-arm PEG acrylate-PEG dithiol SN; B) 8-arm PEG acrylate-DTT with alginate DN and 8-arm PEG acrylate-DTT.

3.4. Tensile test and compression test of cryogels

In the tensile test, when the applied force increased, the trend changed from an upward to a flat trend, indicating that the cryogel was stretched to the endurance limit and broke. From the tensile test analysis, it can be seen that SN cryogels break at a greater tensile force, so they have stronger mechanical properties (**Figure 8**). The elastic and compressive properties of cryogels are determined by applying physical stress to the gel, which in turn is used to calculate Young's modulus, which is a mathematical description of the tendency of an object or substance to deform when a force is applied to it. **Figure 8** shows the tensile Young's modulus of each cryogel sample of the same size, calculated by analyzing the stress and strain values for each cryogel. The calculated tensile modulus of 8-arm PEG-DTT with alginate DN cryogels is around 305.5 kPa. This is lower than that of 8-arm PEG-DTT SN cryogels, which show a value of around 738.2 kPa.
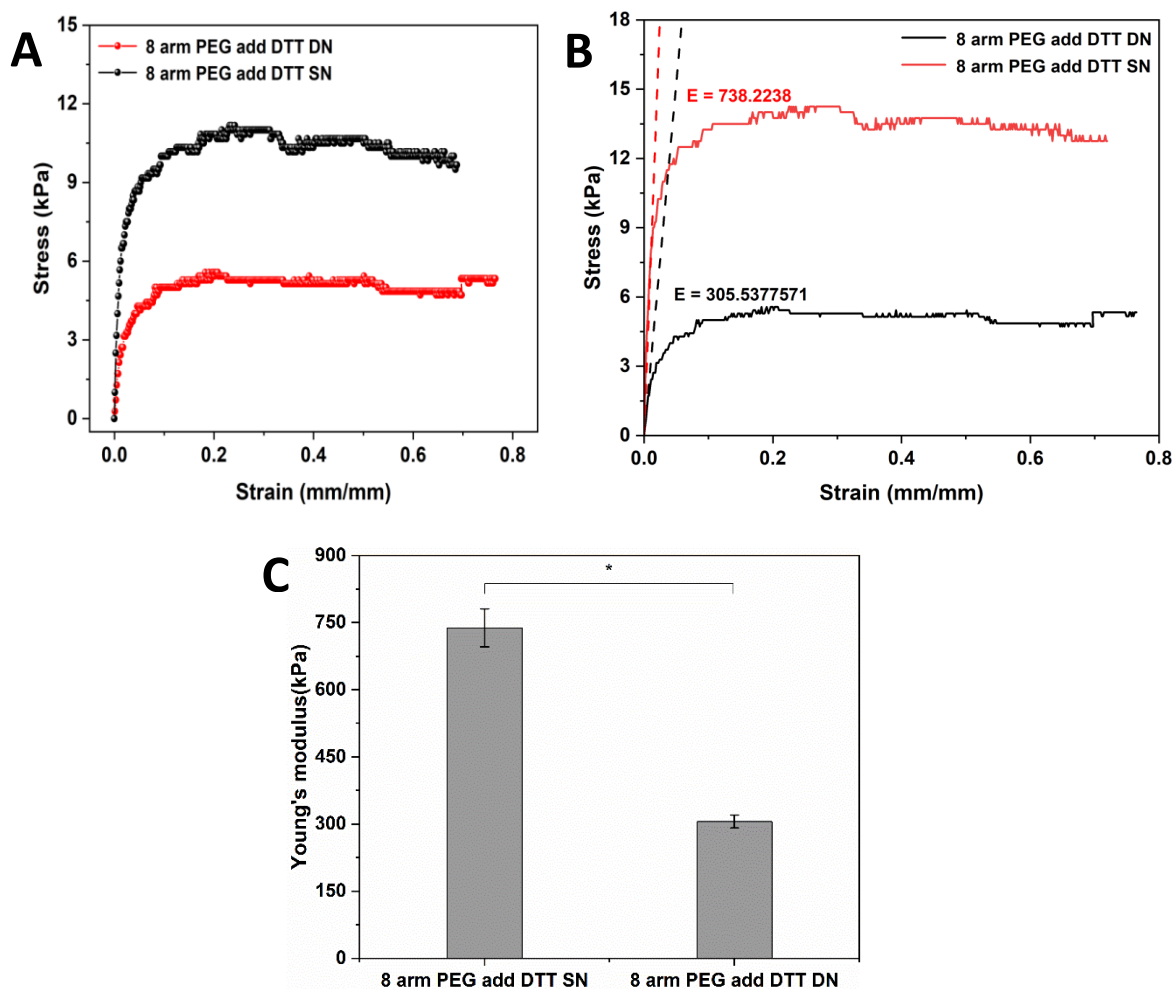
Figure 8. Tensile testing of the cryogels: A) Tensile strength of DN 8-arm PEG -DTT with alginate cryogel and SN 8-arm PEG-DTT. B) Analysis of the tensile test strain-stress data to obtain Young's modulus data. C) Comparison of double network cryogels and single network cryogels tensile test Young's modulus

The compression analysis of hybrid DN cryogels shows a sudden drop from an upward trend, which means that the cryogels when compressed beyond 50% of original length are broken. From the compression test, it can be seen that under the same pressure and deformation, the SN cryogels are not broken, but the DN cryogels have broken (**Figure 9**). 8-arm PEG-DTT with alginate DN cryogels ruptured at 70% strain compared to 8-arm PEG-DTT SN cryogels

which were able to regain shape after compression. It is observed that 8-arm PEG-DTT with alginate DN cryogels require less stress to undergo compression than 8-arm PEG-DTT SN cryogels, suggesting that 8-arm PEG-DTT SN cryogels are more elastic and mechanically stronger, while DN cryogels are mechanical weaker.
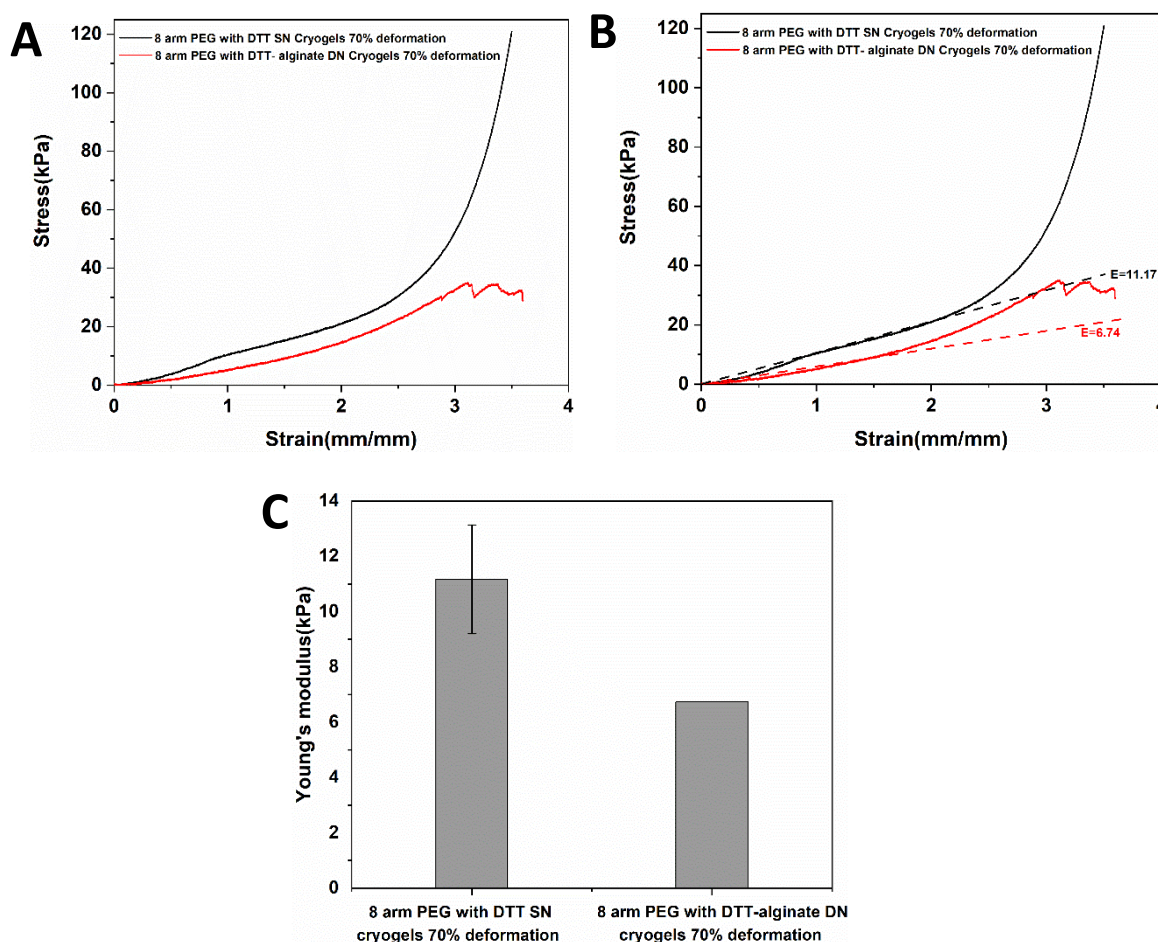
Figure 9. Compression testing of the cryogels. A) Compressive strength of DN 8-arm PEG - DTT with alginate cryogel and SN 8-arm PEG-DTT. B) Analysis of the compressive test strain-stress data to obtain Young's modulus data.

According to the results of the tensile test and compression test, we found that SN cryogels have higher tensile and elastic modulus than the DN cryogel. This may be related to the difference in porosity and pore network in DN cryogel and SN cryogel. At the same time, the

addition of alginate may affect the mechanical properties of DN cryogels to some extent and the mechanical strength of DN cryogels prepared with alginate may be insufficient.

3.5. Swelling kinetics and degradation rate of cryogels

The swelling kinetics of SN and DN cryogels is shown in **Figure 10**. In the test, the time required to reach equilibrium value of water uptake capacity was determined for each cryogel. All SN and DN cryogels reach > 80% W_u in 2 min after incubation in the aqueous buffer. Both SN and respective DN cryogels have similar swelling kinetics and all cryogels reach close to equilibrium swelling within 30 min. After 30 min, the change in the water uptake capacity of cryogels is minimal. The water uptake capacity of 8-arm PEG acrylate-DTT cryogels always remains at the same level of 89% after 2 min. The water uptake capacity of 8 arm PEG acrylate with SH-PEG-SH cryogels is moderate in the initial stage, and the water uptake capacity gradually increases over time but the equilibrium swelling time remains 30 min. The water uptake capacity of 8-arm PEG Acrylate + DTBA cryogels was slowest in the initial stage, and it increased rapidly over time, and reached to 88% Wu at 24 h. The differences in the swelling kinetics of the cryogels indicate differences in the pore interconnectivity and crosslinking density/efficiency. A faster swelling equilibrium but comparatively lower W_u in 8-arm PEG-DTT DN and SN gels shows higher crosslinking density of the gels with a highly interconnected pore network, which facilitates faster water uptake in the network. Conversely, slower water uptake in 8-arm PEG-DTBA DN and SN gels show high crosslink density and lower pore interconnectivity which decreases the water uptake rate. Nonetheless, the faster equilibration of the cryogels with the surrounding medium makes them an excellent scaffold for cell culture. The faster swelling kinetics indicates pore interconnectivity and an open pore

structure. Both features facilitate cell infiltration as well homogenous transport of the nutrients within the scaffold.
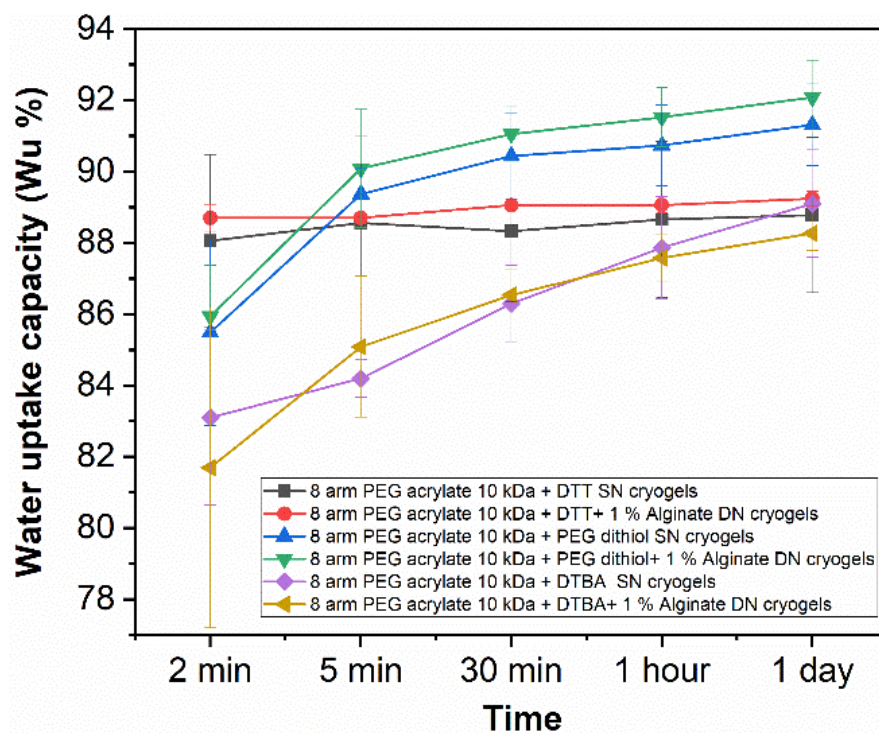
Figure 10. Water uptake capacity of different DN and SN cryogels.

Degradation kinetics of cryogels was studied in phosphate buffer at room temperature. **Figure 11A** shows the degradation of different DN cryogels in the presence of 10 mM EDTA in the medium incubated at room temperature. 4-arm PEG acrylate-DTT with alginate cryogel seemingly has a faster degradation rate than 8-arm PEG cryogels. However, after degrading to 25% the rate of degradation becomes extremely slow. Among 8-arm PEG acrylate cryogels , DN cryogels with DTBA as a crosslinker has the slowest degradation rate while the dithiol containing 8-arm PEG acrylate gels have the fastest degradation. Nonetheless, cryogel degradation is ~5-25% in over 25 days, which is much slower than expected. Previous studies of PEG hydrogel using these dithiol crosslinker shows a degradation time of 8 to 20 days for 4-arm PEG acrylate hydrogels. Thus, based on these reported times, we expected significant

degradation of the cryogels when incubated in PBS at room temperature. To understand the differences in expected degradation time from observed degradation time, we further conducted degradation studies using a few of the DN hydrogels (**Figure 11 B**). In these studies, in order to simulate similar conditions to cryogels, the hydrogels were dried completely and then incubated in the PBS with 2 mM $CaCl_2$. We observed that the DN hydrogels absorbed slowly and the degradation increased gradually over a period of 25 days. However, unexpectedly, the DN hydrogels only degrade by 25% in 25 days. We believe this is due to slow penetration of water into the network and presence of alginate in DN. Both decreased the rate of degradation at room temperature. Lastly, the cryogels' degradation was accelerated when incubated in FBS containing medium at 37 °C. We observed that on day 15, 4-arm PEG-DTT with alginate DN cryogels and a small portion of the 8 arm PEG-DTBA with alginate DN cryogels degraded. On day 18, most of the 8-arm PEG-DTBA with alginate DN cryogels and a small part of the 8-arm PEG-DTBA SN cryogels were degraded. On day 21, most of the 8-arm PEG-DTBA SN cryogels were degraded. A small fraction of 8- arm PEG-PEG dithiol with alginate DN cryogels was degraded on the 24th day, while on Day 27, most of the 8-arm PEG-PEG dithiol with alginate DN cryogels was degraded. Further quantitative studies are required to confirm the degradation rate of the cryogels at 37 °C.
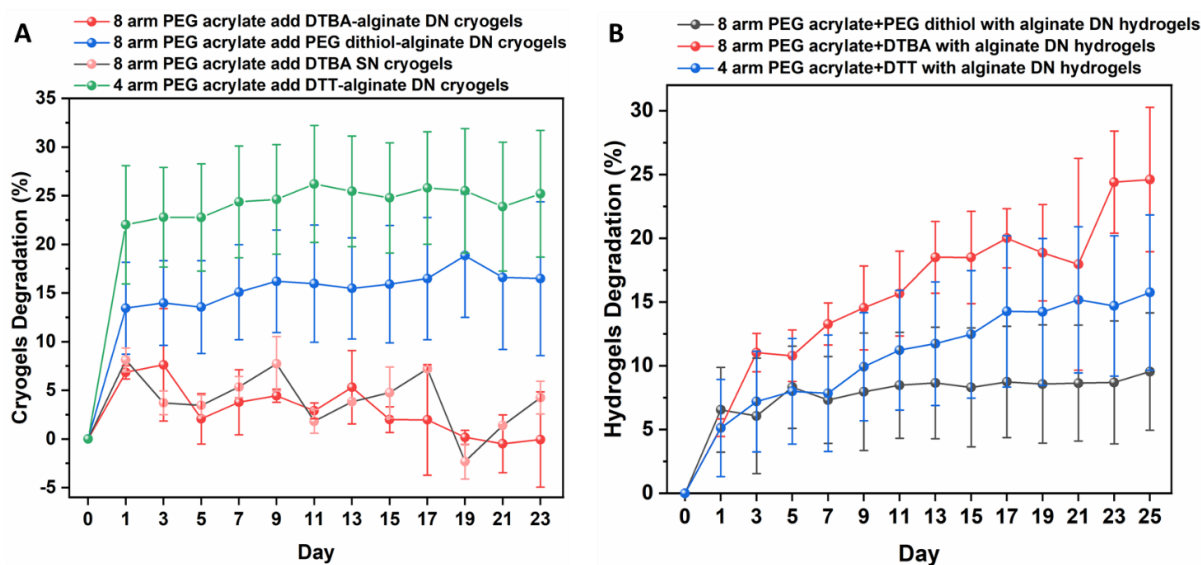
Figure 11. Degradation kinetics of cryogels and hydrogels at room temperature. A) Degradation of cryogels in EDTA containing media; B) Degradation of hydrogels in PBS with 2 mM $CaCl_2$.

3.6. Rheological analysis of DN cryogels

Viscoelastic properties of cryogel were investigated using rheometric measurements (**Figure 12**). By comparing the storage modulus of 8-arm PEG acrylate-DTBA with alginate DN cryogels and 8 arm PEG acrylate-PEG dithiol with alginate DN cryogels, it was found that cryogels with low MW cross-linking agent (DTBA) have higher storage modulus than those using a high MW crosslinker (PEG dithiol). By comparing the storage moduli of 8 arm PEG acrylate-PEG dithiol add alginate DN cryogels and 8 arm PEG acrylate-PEG dithiol SN cryogels, it was found that the storage modulus of SN cryogels is higher than that of DN cryogels. Our results show that both the chemical structure and the crosslinker MW affect the storage modulus of the resulting hydrogels.
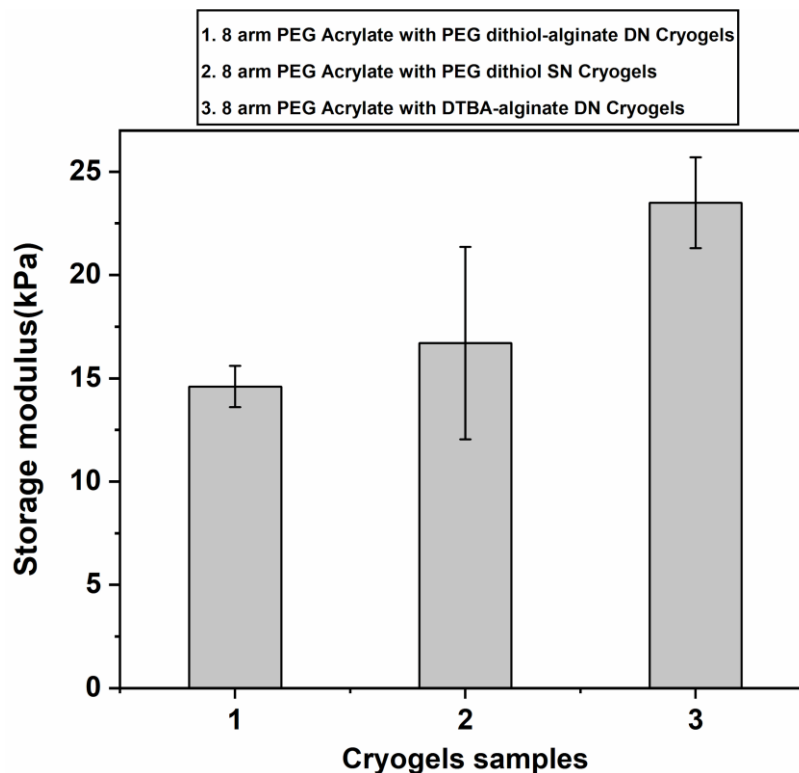
Figure 12. Cryogels sample storage modulus data.

3.7. sGAG synthesis by chondrocytes in cryogel constructs.

The standard curve for chondroitin sulfate standard showed linear correlation between increasing chondroitin sulfate concentration and the OD_{525} ($R^2=0.99$). The DMMB assay was conducted at pH 1.5 to avoid interference from alginate in sGAG readout due to similarity in structure and ability to react with the dye. Cryogel samples without cells were included as negative controls to ensure the degree of interference if any from alginate in DMBB assay readouts. The OD at 525 nm from control cryogels samples of 4 arm PEG-DTT with alginate DN cryogels and 8 arm PEG-SH-PEG-SH with alginate DN cryogels was close to baseline indicating negligible interference of alginate in the assay. In cryogels co-cultured with chondrocytes, the average concentration of 50.48 µL/ml in 8-arm PEG -DTBA with alginate DN cryogels (**Figure 13**). While the average concentration sGAG was 24.42 µL/ml and 22.30µL/ml for 8 arm PEG -DTBA SN cryogels is, and 8 arm PEG –PEG dithiol with alginate

DN cryogels respectively. The 4 arm PEG -DTT with alginate DN cryogels showed the lowest amount of sGAG accumulation with an average concentration of 11.70 µg/ml. The chondrocytes cultured on TCPS were included as positive control and secreted about 19.27µg/ml sGAG during the test period. The experiment shows that macroporisty played an important role in increasing sGAG secretion as the sGAG secretion was highest in 8-arm PEG acrylate DN cryogels compared 4-arm acrylate DN cryogels which were non-porous in nature. However, further normalization of the data to the cell number or DNA content is required before making any further conclusions. Additionally, the difference in mechanical properties of cryogels also needs to established to conclusively determine the role of porosity in ECM accumulation.

Figure 13. A) Chondroitin sulfate standards; B) Concentration of sGAGs in different kinds of cryogels.
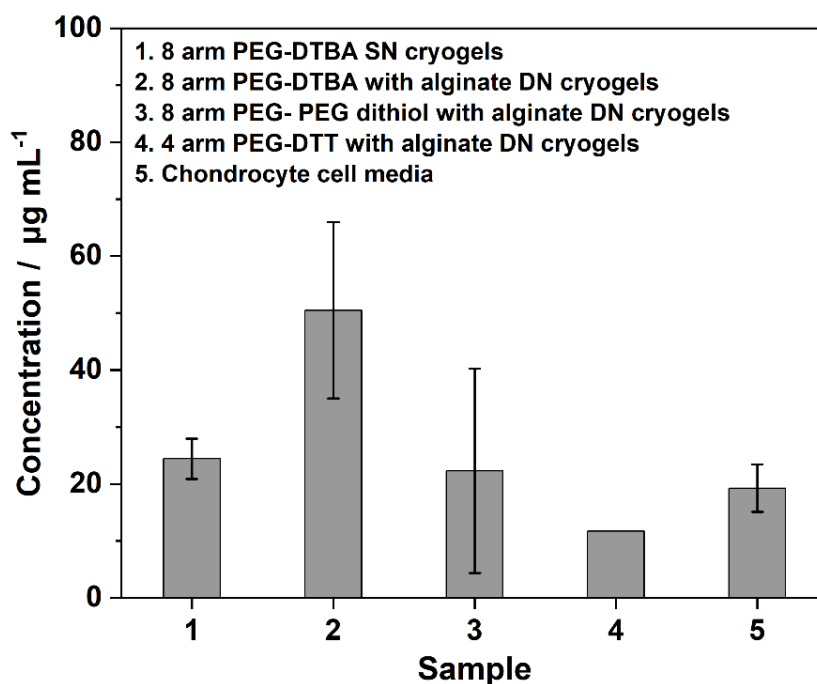
4. Limitations of the Study

In this study, we combined 4 arm PEG acrylate/ 8 arm PEG acrylate with alginate to synthesize hybrid DN cryogels. The goal was to generate a tough interconnected porous network to be used as a substrate chondrocyte culture, and eventually cartilage repair. By modifying the various conditions of synthesis such as temperature, concentration of monomers and their molecular weight, we established conditions which generated macroporous cryogels. One of the novelties the cryogels generated in the study is use of chemical reactions which are non-toxic and do not generate any harmful chemical initiators. Previous studies used these polymer combinations to generate a DN employed free radical polymerization which required toxic initiators for crosslinking reactions.

After successfully establishing the conditions for cryogel synthesis, a series of characterizations were performed on DN cryogels. These characterizations revealed the macroporous structure, a fast-swelling rate, a very slow degradation rate and mechanical properties of DN cryogels. However, some of the methods used for characterization as well as sample size included in these characterizations were not appropriate. Thus, we have identified some specific limitations for each of the characterizations and identified what future work is required to establish conclusive data for each property. Some of the specific revisions to each of the methods in the current work are described below.

A.   Pore size quantification and pore interconnectivity measurements

The pore size of the synthesized cryogel was estimated based on the SEM images. The primary deficiency here is that pore size range was not measured accurately. Further only the upper and lower surfaces of the cryogels were photographed with SEM, and a cross-sectional image of cryogels was not obtained. Estimation of pore size by SEM imaging is very approximate and thus, measuring pore size across replicate samples for different cryogels is

required to establish an accurate pore size range. We will also get additional SEM images of the cross-sectional surface of cryogels to establish the presence of pores throughout the network. We will use Image J to measure pore size across different cryogel samples. Briefly, each image will be thresholded in Image J and the scale bar will be calibrated to image pixel size. 100 random pore diameters and areas will be determined by measuring the long diameter of each pore and tracing the outer edge of the pore, respectively. The average pore sizes from three replicate samples for each type of cryogel will then be reported. We will also determine the distribution of pore sizes in different cryogels and the pore sizes of cryogels prepared using different cross-linking agents will be further compared.

The presence of an interconnected open porous network in cryogels was indirectly deduced from the fast-swelling rate and short swelling equilibration times. However, to establish pore interconnectivity experimentally, we need to perform a set of experiments. First, we can study protein diffusion through cryogels and determine their relative diffusivity in cryogels. If the protein diffusivity in cryogels is equivalent to their diffusivity in the water, this can be an indirect measurement of the high porosity of cryogels. It also means that the pores are highly interconnected, which provides a continuous network of the aqueous medium in which the protein can diffuse. In a second experiment, we can determine the hydraulic permeability of the cryogels. Hydraulic permeability will allow us to characterize the convective transport of the water through cryogels. If the cryogels form a continuous network of capillaries due to pore interconnectivity the hydraulic permeability of the cryogels will be high.

B. Mechanical testing of cryogels

In the following study, we characterized various tensile and compressive properties of cryogels in order to establish their application for cartilage tissue engineering. For both tensile and compressive tests, hybrid DN cryogels formed using different dithiol crosslinkers (DTT, DTBA and PEG dithiol) and were included for comparative analysis. Further, a sample size of

3 was required for each of the cryogels. A major flaw for both of the tests was that cryogels were not pre-equilibrated in the buffer before testing. Thus, all tests should be repeated where the sample is equilibrated in buffer for 2- 4h and then the compression or tensile test should be performed.

The tensile test was performed on cylindrical samples. However, as per ASTM standards and current standard methods for tensile testing the sample should have been dumbbell shaped. Thus, the experiments should be repeated using dumbbell shaped cryogel samples. The sample dimension for tensile testing according to ASTM-D638-V will have a length 63.5mm, width 9.53mm, gauge length 9.53mm, gauge width 3.18mm (**Figure 14**)
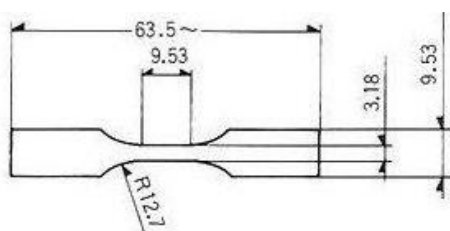
Figure 14. Dimension of dumbbell shaped sample for tensile testing of cryogel samples.

To conduct the tensile testing on cryogels the samples will be cut into dumbbell shapes with the dimensions described above. The samples will be equilibrated in a buffer for 2-4 h and then positioned in a uniaxial tensile tester with a load cell of 25 N. In the previous data the rate of applied stress was relatively fast, which may have influenced the quality of the data we collected. Thus, in the proposed set of experiments we will run the tensile test at 5 mm/min. The scaffold thickness and grip distance will be measured and taken into account before testing the sample. A stress-strain curve so generated will be used for analysis. The linear region of the curve will be used to derive the Youngs modulus of the cryogels samples. To maintain uniformity, the linear region of the curve will be analyzed at a 10% strain across all samples and replicates.

Compression testing procedures for cryogels in future experiments will be done as described in the Materials and Methods section, but with a few changes. The load cell used for these studies will be 100 N and force will be applied at a rate of 5 mm/min up to 70% compression. The samples will be pre-equilibrated in buffer before testing. The linear region of the stress strain curve will be analyzed at 10% strain to obtain Youngs modulus.

Lastly, for determining the storage modulus of the cryogels, the cryogels will be pre-soaked into buffer and then used for analysis. Additional samples of cryogels with different crosslinkers will be consistently included across all tests.

C. Analysis of sGAG secretion in cryogel constructs

The data included for sGAG quantification across different samples of cryogels needs to be normalized to DNA content across each sample. We will analyze the lysate from each sample using a pic-green assay to account for variation in cell number across samples and to normalize the value of sGAG secretion. The normalized data can then be used for reaching further conclusions and for the design of experiments.

5. Future work

Future studies will focus on improving the mechanical strength of the DN cryogels. We will test different experimental conditions to achieve this goal. To strengthen the cryogels, we will: 1) use new crosslinkers; 2) change the concentration of polymers and crosslinkers; and 3) repeat freeze thaw cycles. Next, I hope to test the injectability of these cryogels. We will also conduct a series of biological tests to test chondrocyte behavior when cultured on these cryogel scaffolds. Finally, the optimized cryogels performance will be tested in an animal model cartilage defect (**Figure 15**).
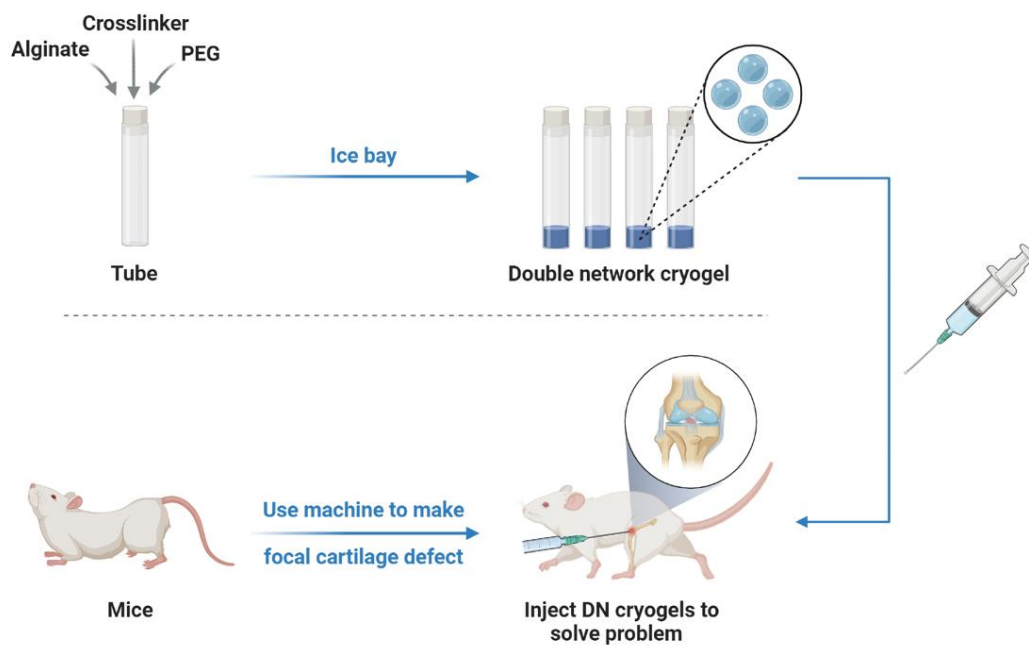
Figure 15. Future works for making cryogel to repair cartilage defect.

Chapter 2

Developing Mice Model of Post Traumatic Osteoarthritis

1. Introduction

After suffering a traumatic joint injury (such as anterior cruciate ligament (ACL) or meniscal injury), approximately half of patients will continue to develop post-traumatic osteoarthritis (PTOA) within 10-20 years.[104-105] This increases the risk of OA development not only in older age groups, but in young people or athletes who suffer from traumatic joint injuries. The research on PTOA[106] has been highly valued by scientists. The newly developed PTOA non-invasive tibial compression model developed by scientists in recent years can accurately capture some of the characteristics of traumatic joint injuries that are typically found in PTOA in humans. The non-invasive model can use externally applied mechanical loads to simulate a traumatic injury without the need for surgical intervention. Therefore, the non-invasive injury model is completely sterile, avoiding potential infections and other problems caused by the trauma of surgery/invasive injury surgery.[107] After tibial compression, the knee joint shows increased anterior and posterior joint laxity.[108] Synovial inflammation occurs within 3-5 days after injury and lasts for 8 weeks.[109-110] In addition, it has been reported that the intracellular activation of NF-κB in cartilage occurs 12 hours after mechanical injury in the PTOA mouse model.[111] It is well established that NF-κB activation plays a crucial role in the early development of PTOA and regulates inflammation. Here in this study, we established the non-invasive tibial compression mouse model of PTOA. We characterized anterior-posterior joint laxity post loading to establish the reproducibility of our method.

2. Materials and methods

2.1. Anterior cruciate ligament rupture using cyclic mechanical loading

We obtained freshly sacrificed mice (male, 9-12 weeks old, n=20) from the animal facility. The cadaveric mice knees were then mechanically loaded on randomly assigned knee joints to induce anterior cruciate ligament (ACL) rupture using the Instron machine. Briefly, mice cadavers were laid flat on a platform, and then the mice knees were positioned at 90 degrees in a 3 points bending mode between two customized cups. Each cup was designed to hold the knee and paw respectively. Thus, one cup was arc-shaped, and the other end was wedge-shaped (**Figure 17**) 40 sets of mice knee joints underwent cyclic mechanical overload (12N axial compression load for 60 cycles). The mice were randomly assigned to three groups including a sham control (CTRL, n = 6), joint injury (INJ, n = 13). Only one of the knees underwent mechanical loading in each mouse while tbe others were used as contralateral controls. Post mechanical loading, the hind limbs were dissected, and three unknown investigators rated anterior and posterior laxity (0 = naive, 1 = increased anterior and posterior laxity). The total score for each joint was calculated, and the CTRL and INJ joint scores were compared using the Mann-Whitney test.[112]
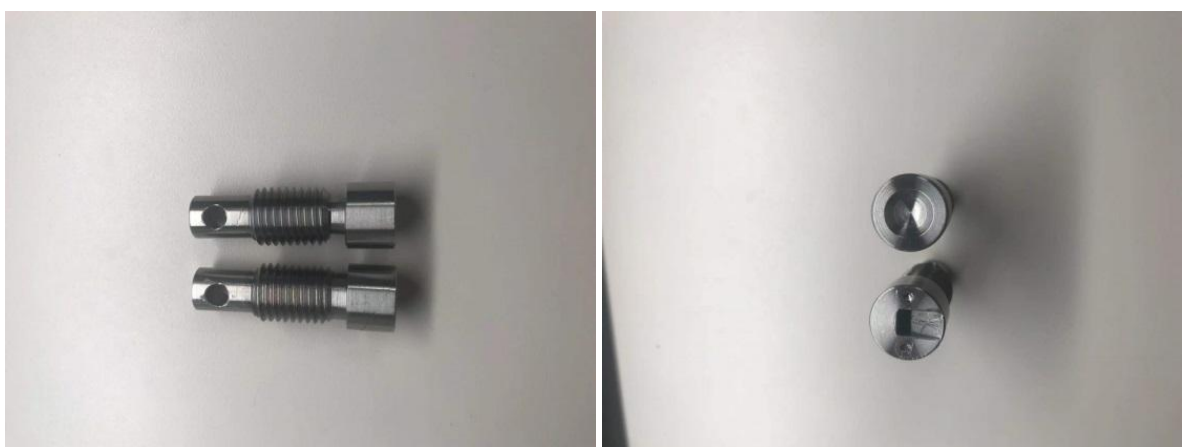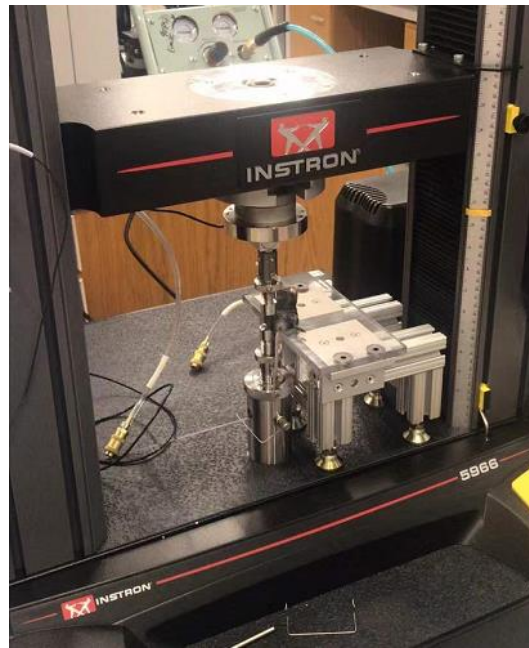
Figure 16. The shape of the screws and the diagram of the instron machine that destroys the mice joint.

3. Results

3.1. Laxity test

The cyclic mechanical loading of the cadaveric mice knee joint consistently induced ACL rupture. This was evident from the force displacement curve whereby a pop sound was heard upon ACL rupture and a drop in the force displacement curve occurred. The induction of ACL ruptures by mechanical loading was also confirmed by conducting the laxity test. The three blinded investigators reported a score zero for 10 knees, a score of 1 for 3 knees, and a score of 3 for 19 knees (**Figure 18**). Some of the knees were excluded from analysis as the femur of was damaged when the mice joint was mechanically loaded. The laxity test further established that the mechanical overload can reproducibly induce ACL rupture. This indicated the suitability of the method for induction of ACL ruptures and using this method to establish mouse models of PTOA via non-invasive trauma to the joint.
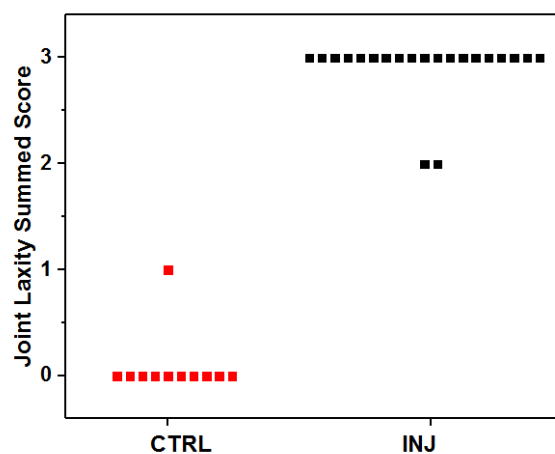
Figure 17. Average Laxity test scores reported by three blinded investigators.

4. Conclusion

In animal experiments, laxity tests proved that mechanical loading led to an increase in joint laxity, indicating ACL rupture. We conclude that this method can reliably be used to establish a non-invasive mouse model of PTOA. Our results are in line with previous reported studies which used a similar model of PTOA.[109, 113] Further studies will include pain measurements and histological analysis to monitor development and progression of PTOA in mouse models after ACL-rupture.

References

1. Buckwalter, J.; Mankin, H. J. J. o. B.; surgery, j., Articular cartilage: part I. .*Journal of Bone and Joint Surgery* **1997,** *79* (4), 600.

2. Sophia Fox, A. J.; Bedi, A.; Rodeo, S. A. J. S. h., The basic science of articular cartilage: structure, composition, and function. *SAGE open medicine* **2009,** *1* (6), 461-468.

3. Buckwalter, J. A.; Mankin, H. J.; Grodzinsky, A. J. J. I. C. L.-A. A. o. O. S., Articular cartilage and osteoarthritis. *Instr. Course Lect.* **2005,** *54*, 465.

4. Matsiko, A.; Levingstone, T. J.; O'Brien, F. J. J. M., Advanced strategies for articular cartilage defect repair. *Materials* **2013,** *6* (2), 637-668.

5. Mink, J. H.; Deutsch, A. L. J. R., Occult cartilage and bone injuries of the knee: detection, classification, and assessment with MR imaging. *radiology* **1989,** *170* (3), 823-829.

6. Hjelle, K.; Solheim, E.; Strand, T.; Muri, R.; Brittberg, M. J. A. T. J. o. A.; Surgery, R., Articular cartilage defects in 1,000 knee arthroscopies. *Arthroscopy - Journal of Arthroscopic and Related Surgery* **2002,** *18* (7), 730-734.

7. Hunziker, E. B. J. C. O.; Research®, R., Biologic repair of articular cartilage: defect models in experimental animals and matrix requirements. *Clinical Orthopaedics and Related Research* **1999,** *367*, S135-S146.

8. Curl, W. W.; Krome, J.; Gordon, E. S.; Rushing, J.; Smith, B. P.; Poehling, G. G., Cartilage injuries: A review of 31,516 knee arthroscopies. *Arthroscopy* **1997,** *13* (4), 456-460.

9. Widuchowski, W.; Widuchowski, J.; Trzaska, T., Articular cartilage defects: Study of 25,124 knee arthroscopies. *Knee* **2007,** *14* (3), 177-182.

10. Cui, A.; Li, H.; Wang, D.; Zhong, J.; Chen, Y.; Lu, H. J. E., Global, regional prevalence, incidence and risk factors of knee osteoarthritis in population-based studies. *Lancet* **2020,** *29*, 100587.

11. Cossey, A. J.; Spriggins, A. J. J. T. J. o. a., The use of computer-assisted surgical navigation to prevent malalignment in unicompartmental knee arthroplasty. *Journal of Arthroplasty* **2005,** *20* (1), 29-34.

12. Baumgaertner, M. R.; Cannon Jr, W.; Vittori, J. M.; Schmidt, E. S.; Maurer, R. C. J. C. o.; research, r., Arthroscopic debridement of the arthritic knee. *Clin. Orthop. Relat. Res.* **1990,** (253), 197-202.

13. Migliorini, F.; Maffulli, N.; Baroncini, A.; Knobe, M.; Tingart, M.; Eschweiler, J. J. B. m. b., Matrix-induced autologous chondrocyte implantation versus autologous matrix-induced chondrogenesis for chondral defects of the talus: a systematic review. *British medical bulletin* **2021**.

14. Specialists, N. O. Cartilage Defects of the Knee. https://www.newenglandorthopedics.com/knee-treatments/cartilage-defects-knee/.

15. McCormick, F.; Harris, J. D.; Abrams, G. D.; Frank, R.; Gupta, A.; Hussey, K.; Wilson, H.; Bach, B.; Cole, B., Trends in the Surgical Treatment of Articular Cartilage Lesions in the United States: An Analysis of a Large Private-Payer Database Over a Period of 8 Years. *Arthroscopy* **2014,** *30* (2), 222-226.

16. Martin, A. R.; Patel, J. M.; Zlotnick, H. M.; Carey, J. L.; Mauck, R. L., Emerging therapies for cartilage regeneration in currently excluded 'red knee' populations. *Npj Regen Med* **2019,** *4*.

17. Griffith, L. G.; Naughton, G. J. s., Tissue engineering--current challenges and expanding opportunities. *Science* **2002,** *295* (5557), 1009-1014.

18. Huang, B. J.; Hu, J. C.; Athanasiou, K. A. J. B., Cell-based tissue engineering strategies used in the clinical repair of articular cartilage. *Biomaterials* **2016,** *98*, 1-22.

19. Nuernberger, S.; Cyran, N.; Albrecht, C.; Redl, H.; Vecsei, V.; Marlovits, S., The influence of scaffold architecture on chondrocyte distribution and behavior in matrix-associated chondrocyte transplantation grafts. *Biomaterials* **2011,** *32* (4), 1032-40.

20. Dehne, T.; Karlsson, C.; Ringe, J.; Sittinger, M.; Lindahl, A., Chondrogenic differentiation potential of osteoarthritic chondrocytes and their possible use in matrix-associated autologous chondrocyte transplantation. *Arthritis Res Ther* **2009,** *11* (5), R133.

21. Mouw, J. K.; Connelly, J. T.; Wilson, C. G.; Michael, K. E.; Levenston, M. E., Dynamic compression regulates the expression and synthesis of chondrocyte-specific matrix molecules in bone marrow stromal cells. *Stem Cells* **2007,** *25* (3), 655-63.

22. Huey, D. J.; Hu, J. C.; Athanasiou, K. A., Unlike bone, cartilage regeneration remains elusive. *Science* **2012,** *338* (6109), 917-21.

23. Bas, O.; De-Juan-Pardo, E. M.; Meinert, C.; D'Angella, D.; Baldwin, J. G.; Bray, L. J.; Wellard, R. M.; Kollmannsberger, S.; Rank, E.; Werner, C.; Klein, T. J.; Catelas, I.; Hutmacher, D. W., Biofabricated soft network composites for cartilage tissue engineering. *Biofabrication* **2017,** *9* (2), 025014.

24. Vinatier, C.; Guicheux, J., Cartilage tissue engineering: From biomaterials and stem cells to osteoarthritis treatments. *Ann Phys Rehabil Med* **2016,** *59* (3), 139-144.

25. Herring, M. J.; Rud, C. T.; Macalena, J. A., Autologous Chondrocyte Implantation Using a Bilayer Collagen Membrane with Bone Graft and Anteromedialization of the Tibial Tubercle for the Treatment of a Large Osteochondral Defect in the Lateral Knee Trochlea: A Case Report. *JBJS Case Connect* **2016,** *6* (2), e35.

26. Vijayan, S.; Bartlett, W.; Bentley, G.; Carrington, R. W.; Skinner, J. A.; Pollock, R. C.; Alorjani, M.; Briggs, T. W., Autologous chondrocyte implantation for osteochondral lesions in the knee using a bilayer collagen membrane and bone graft: a two- to eight-year follow-up study. *J Bone Joint Surg Br* **2012,** *94* (4), 488-92.

27. Gigante, A.; Enea, D.; Greco, F.; Bait, C.; Denti, M.; Schonhuber, H.; Volpi, P., Distal realignment and patellar autologous chondrocyte implantation: mid-term results in a selected population. *Knee Surg Sports Traumatol Arthrosc* **2009,** *17* (1), 2-10.

28. Ochi, M.; Uchio, Y.; Kawasaki, K.; Wakitani, S.; Iwasa, J., Transplantation of cartilage-like tissue made by tissue engineering in the treatment of cartilage defects of the knee. *J Bone Joint Surg Br* **2002,** *84* (4), 571-8.

29. Kuroda, R.; Ishida, K.; Matsumoto, T.; Akisue, T.; Fujioka, H.; Mizuno, K.; Ohgushi, H.; Wakitani, S.; Kurosaka, M., Treatment of a full-thickness articular cartilage defect in the femoral condyle of an athlete with autologous bone-marrow stromal cells. *Osteoarthritis Cartilage* **2007,** *15* (2), 226-31.

30. Steinwachs, M.; Cavalcanti, N.; Mauuva Venkatesh Reddy, S.; Werner, C.; Tschopp, D.; Choudur, H. N., Arthroscopic and open treatment of cartilage lesions with BST-CARGEL scaffold and microfracture: A cohort study of consecutive patients. *Knee* **2019,** *26* (1), 174-184.

31. Steinwachs, M. R.; Waibl, B.; Mumme, M., Arthroscopic Treatment of Cartilage Lesions With Microfracture and BST-CarGel. *Arthrosc Tech* **2014,** *3* (3), e399-402.

32. Brix, M. O.; Stelzeneder, D.; Trattnig, S.; Windhager, R.; Domayer, S. E., Cartilage repair of the knee with Hyalograft C:(R) magnetic resonance imaging assessment of the glycosaminoglycan content at midterm. *Int Orthop* **2013,** *37* (1), 39-43.

33. Eshed, I.; Trattnig, S.; Sharon, M.; Arbel, R.; Nierenberg, G.; Konen, E.; Yayon, A., Assessment of cartilage repair after chondrocyte transplantation with a fibrin-hyaluronan matrix--correlation of morphological MRI, biochemical T2 mapping and clinical outcome. *Eur J Radiol* **2012,** *81* (6), 1216-23.

34. Nehrer, S.; Domayer, S.; Dorotka, R.; Schatz, K.; Bindreiter, U.; Kotz, R., Three-year clinical outcome after chondrocyte transplantation using a hyaluronan matrix for cartilage repair. *Eur J Radiol* **2006,** *57* (1), 3-8.

35. Wasyłeczko, M.; Sikorska, W.; Chwojnowski, A. J. M., Review of synthetic and hybrid scaffolds in cartilage tissue engineering. *Membranes* **2020,** *10* (11), 348.

36. Ngadimin, K. D.; Stokes, A.; Gentile, P.; Ferreira, A. M., Biomimetic hydrogels designed for cartilage tissue engineering. *Biomater Sci* **2021,** *9* (12), 4246-4259.

37. He, A.; Liu, L.; Luo, X.; Liu, Y.; Liu, Y.; Liu, F.; Wang, X.; Zhang, Z.; Zhang, W.; Liu, W.; Cao, Y.; Zhou, G., Repair of osteochondral defects with in vitro engineered cartilage based on autologous bone marrow stromal cells in a swine model. *Sci Rep* **2017,** *7*, 40489.

38. Zhang, Y.; Yang, F.; Liu, K.; Shen, H.; Zhu, Y.; Zhang, W.; Liu, W.; Wang, S.; Cao, Y.; Zhou, G., The impact of PLGA scaffold orientation on in vitro cartilage regeneration. *Biomaterials* **2012,** *33* (10), 2926-35.

39. Ossendorf, C.; Kaps, C.; Kreuz, P. C.; Burmester, G. R.; Sittinger, M.; Erggelet, C., Treatment of posttraumatic and focal osteoarthritic cartilage defects of the knee with autologous polymer-based three-dimensional chondrocyte grafts: 2-year clinical results. *Arthritis Res Ther* **2007,** *9* (2), R41.

40. Conoscenti, G.; Schneider, T.; Stoelzel, K.; Carfi Pavia, F.; Brucato, V.; Goegele, C.; La Carrubba, V.; Schulze-Tanzil, G., PLLA scaffolds produced by thermally induced phase separation (TIPS) allow human chondrocyte growth and extracellular matrix formation dependent on pore size. *Mater Sci Eng C Mater Biol Appl* **2017,** *80*, 449-459.

41. Varghese, S.; Hwang, N. S.; Canver, A. C.; Theprungsirikul, P.; Lin, D. W.; Elisseeff, J., Chondroitin sulfate based niches for chondrogenic differentiation of mesenchymal stem cells. *Matrix Biol* **2008,** *27* (1), 12-21.

42. Zhao, X.; Papadopoulos, A.; Ibusuki, S.; Bichara, D. A.; Saris, D. B.; Malda, J.; Anseth, K. S.; Gill, T. J.; Randolph, M. A., Articular cartilage generation applying PEG-LA-DM/PEGDM copolymer hydrogels. *BMC Musculoskelet Disord* **2016,** *17*, 245.

43. Grad, S.; Kupcsik, L.; Gorna, K.; Gogolewski, S.; Alini, M., The use of biodegradable polyurethane scaffolds for cartilage tissue engineering: potential and limitations. *Biomaterials* **2003,** *24* (28), 5163-71.

44. Oh, S. H.; Kim, T. H.; Im, G. I.; Lee, J. H., Investigation of pore size effect on chondrogenic differentiation of adipose stem cells using a pore size gradient scaffold. *Biomacromolecules* **2010,** *11* (8), 1948-55.

45. Cheng, A.; Schwartz, Z.; Kahn, A.; Li, X.; Shao, Z.; Sun, M.; Ao, Y.; Boyan, B. D.; Chen, H., Advances in Porous Scaffold Design for Bone and Cartilage Tissue Engineering and Regeneration. *Tissue Eng Part B Rev* **2019,** *25* (1), 14-29.

46. Hafezi, M.; Nouri Khorasani, S.; Zare, M.; Esmaeely Neisiany, R.; Davoodi, P., Advanced Hydrogels for Cartilage Tissue Engineering: Recent Progress and Future Directions. *Polymers (Basel)* **2021,** *13* (23).

47. Vega, S. L.; Kwon, M. Y.; Burdick, J. A., Recent advances in hydrogels for cartilage tissue engineering. *Eur Cell Mater* **2017,** *33*, 59-75.

48. Ingavle, G. C.; Frei, A. W.; Gehrke, S. H.; Detamore, M. S., Incorporation of aggrecan in interpenetrating network hydrogels to improve cellular performance for cartilage tissue engineering. *Tissue Eng Part A* **2013,** *19* (11-12), 1349-59.

49. Snyder, T. N.; Madhavan, K.; Intrator, M.; Dregalla, R. C.; Park, D., A fibrin/hyaluronic acid hydrogel for the delivery of mesenchymal stem cells and potential for articular cartilage repair. *J Biol Eng* **2014,** *8*, 10.

50. Arnold, M. P.; Daniels, A. U.; Ronken, S.; Garcia, H. A.; Friederich, N. F.; Kurokawa, T.; Gong, J. P.; Wirz, D., Acrylamide Polymer Double-Network Hydrogels: Candidate Cartilage Repair Materials with Cartilage-Like Dynamic Stiffness and Attractive Surgery-Related Attachment Mechanics. *Cartilage* **2011,** *2* (4), 374-83.

51. Yasuda, K.; Kitamura, N.; Gong, J. P.; Arakaki, K.; Kwon, H. J.; Onodera, S.; Chen, Y. M.; Kurokawa, T.; Kanaya, F.; Ohmiya, Y.; Osada, Y., A novel double-network hydrogel induces spontaneous articular cartilage regeneration in vivo in a large osteochondral defect. *Macromol Biosci* **2009,** *9* (4), 307-16.

52. Kitamura, N.; Yokota, M.; Kurokawa, T.; Gong, J. P.; Yasuda, K., In vivo cartilage regeneration induced by a double-network hydrogel: Evaluation of a novel therapeutic strategy for femoral articular cartilage defects in a sheep model. *J Biomed Mater Res A* **2016,** *104* (9), 2159-65.

53. Ogawa, M.; Kitamura, N.; Kurokawa, T.; Arakaki, K.; Tanaka, Y.; Gong, J. P.; Yasuda, K., Poly(2-acrylamido-2-methylpropanesulfonic acid) gel induces articular cartilage regeneration in vivo: comparisons of the induction ability between single- and double-network gels. *J Biomed Mater Res A* **2012,** *100* (9), 2244-51.

54. Gosset, M.; Berenbaum, F.; Thirion, S.; Jacques, C. J. N. p., Primary culture and phenotyping of murine chondrocytes. **2008,** *3* (8), 1253-1260.

55. Chen, Q.; Chen, H.; Zhu, L.; Zheng, J., Fundamentals of double network hydrogels. *J Mater Chem B* **2015,** *3* (18), 3654-3676.

56. Levett, P. A.; Hutmacher, D. W.; Malda, J.; Klein, T. J., Hyaluronic acid enhances the mechanical properties of tissue-engineered cartilage constructs. *PLoS One* **2014,** *9* (12), e113216.

57. Imabuchi, R.; Ohmiya, Y.; Kwon, H. J.; Onodera, S.; Kitamura, N.; Kurokawa, T.; Gong, J. P.; Yasuda, K., Gene expression profile of the cartilage tissue spontaneously regenerated

in vivo by using a novel double-network gel: comparisons with the normal articular cartilage. *BMC Musculoskelet Disord* **2011,** *12*, 213.

58. Fukui, T.; Kitamura, N.; Kurokawa, T.; Yokota, M.; Kondo, E.; Gong, J. P.; Yasuda, K., Intra-articular administration of hyaluronic acid increases the volume of the hyaline cartilage regenerated in a large osteochondral defect by implantation of a double-network gel. *J Mater Sci Mater Med* **2014,** *25* (4), 1173-82.

59. Sun, J. Y.; Zhao, X.; Illeperuma, W. R.; Chaudhuri, O.; Oh, K. H.; Mooney, D. J.; Vlassak, J. J.; Suo, Z., Highly stretchable and tough hydrogels. *Nature* **2012,** *489* (7414), 133-6.

60. Hong, S.; Sycks, D.; Chan, H. F.; Lin, S.; Lopez, G. P.; Guilak, F.; Leong, K. W.; Zhao, X., 3D Printing of Highly Stretchable and Tough Hydrogels into Complex, Cellularized Structures. *Adv Mater* **2015,** *27* (27), 4035-40.

61. Guo, Z.; Dong, L.; Xia, J.; Mi, S.; Sun, W., 3D Printing Unique Nanoclay-Incorporated Double-Network Hydrogels for Construction of Complex Tissue Engineering Scaffolds. *Adv Healthc Mater* **2021,** *10* (11), e2100036.

62. Guo, Z.; Xia, J.; Mi, S.; Sun, W., Mussel-Inspired Naturally Derived Double-Network Hydrogels and Their Application in 3D Printing: From Soft, Injectable Bioadhesives to Mechanically Strong Hydrogels. *ACS Biomater Sci Eng* **2020,** *6* (3), 1798-1808.

63. Li, X.; Wang, H.; Li, D.; Long, S.; Zhang, G.; Wu, Z., Dual Ionically Cross-linked Double-Network Hydrogels with High Strength, Toughness, Swelling Resistance, and Improved 3D Printing Processability. *ACS Appl Mater Interfaces* **2018,** *10* (37), 31198-31207.

64. Fan, C.; Wang, D. A., Effects of permeability and living space on cell fate and neo-tissue development in hydrogel-based scaffolds: a study with cartilaginous model. *Macromol Biosci* **2015,** *15* (4), 535-45.

65. Chen, G.; Kawazoe, N., Porous Scaffolds for Regeneration of Cartilage, Bone and Osteochondral Tissue. *Adv Exp Med Biol* **2018,** *1058*, 171-191.

66. Okay, O., *Polymeric Cryogels: Macroporous gels with remarkable properties*. Springer: 2014; Vol. 263.

67. Lozinsky, V. J. R. C. B., Polymeric cryogels as a new family of macroporous and supermacroporous materials for biotechnological purposes. *Russian chemical bulletin* **2008,** *57* (5), 1015-1032.

68. Jain, E.; Damania, A.; Shakya, A. K.; Kumar, A.; Sarin, S. K.; Kumar, A., Fabrication of macroporous cryogels as potential hepatocyte carriers for bioartificial liver support. *Colloids Surf B Biointerfaces* **2015,** *136*, 761-71.

69. Jain, E.; Kumar, A., Designing supermacroporous cryogels based on polyacrylonitrile and a polyacrylamide-chitosan semi-interpenetrating network. *J Biomater Sci Polym Ed* **2009,** *20* (7-8), 877-902.

70. Lozinsky, V. I., Cryostructuring of Polymeric Systems. 50.(dagger) Cryogels and Cryotropic Gel-Formation: Terms and Definitions. *Gels* **2018,** *4* (3).

71. Sidorskii, E. V.; Krasnov, M. S.; Yamskova, V. P.; Lozinsky, V. I., Cryostructuring of Polymeric Systems. 57. Spongy Wide-Porous Cryogels Based on the Proteins of Blood Serum: Preparation, Properties and Application as the Carriers of Peptide Bioregulators. *Gels* **2020,** *6* (4).

72. Kumar, A., *Supermacroporous Cryogels: Biomedical and biotechnological applications*. CRC Press: 2016.

73. Qi, C.; Yan, X.; Huang, C.; Melerzanov, A.; Du, Y. J. P.; cell, Biomaterials as carrier, barrier and reactor for cell-based regenerative medicine. *protein & cell* **2015,** *6* (9), 638-653.

74. Lozinsky, V.; Plieva, F. J. E.; technology, m., Poly (vinyl alcohol) cryogels employed as matrices for cell immobilization. 3. Overview of recent research and developments. *Enzyme and Microbial Technology* **1998,** *23* (3-4), 227-242.

75. Hassan, C. M.; Peppas, N. A. J. B. P. h., anionic polymerisation nanocomposites, Structure and applications of poly (vinyl alcohol) hydrogels produced by conventional crosslinking or by freezing/thawing methods. **2000,** 37-65.

76. Lozinsky, V. I. J. R. C. R., Cryotropic gelation of poly (vinyl alcohol) solutions. *Russian Chemical Reviews* **1998,** *67* (7), 573-586.

77. Varfolomeyev, S.; Rainina, E.; Lozinsky, V. J. P.; chemistry, a., Cryoimmobilized enzymes and cells in organic synthesis. *Pure and Applied Chemistry* **1992,** *64* (8), 1193-1196.

78. Lozinsky, V. I.; Galaev, I. Y.; Plieva, F. M.; Savina, I. N.; Jungvid, H.; Mattiasson, B. J. T. i. B., Polymeric cryogels as promising materials of biotechnological interest. *trends in biotechnology* **2003,** *21* (10), 445-451.

79. Bloch, K.; Vanichkin, A.; Damshkaln, L.; Lozinsky, V.; Vardi, P. J. A. b., Vascularization of wide pore agarose–gelatin cryogel scaffolds implanted subcutaneously in diabetic and non-diabetic mice. *Acta Biomater.* **2010,** *6* (3), 1200-1205.

80. Bencherif, S. A.; Sands, R. W.; Bhatta, D.; Arany, P.; Verbeke, C. S.; Edwards, D. A.; Mooney, D. J. J. P. o. t. N. A. o. S., Injectable preformed scaffolds with shape-memory properties. **2012,** *109* (48), 19590-19595.

81. Bhat, S.; Tripathi, A.; Kumar, A., Supermacroprous chitosan-agarose-gelatin cryogels: in vitro characterization and in vivo assessment for cartilage tissue engineering. *J R Soc Interface* **2011,** *8* (57), 540-54.

82. Kathuria, N.; Tripathi, A.; Kar, K. K.; Kumar, A., Synthesis and characterization of elastic and macroporous chitosan-gelatin cryogels for tissue engineering. *Acta Biomater* **2009,** *5* (1), 406-18.

83. Nikhil, A.; Kumar, A., Evaluating potential of tissue-engineered cryogels and chondrocyte derived exosomes in articular cartilage repair. *Biotechnol Bioeng* **2022,** *119* (2), 605-625.

84. Srivastava, A.; Kumar, A., Thermoresponsive poly(N-vinylcaprolactam) cryogels: synthesis and its biophysical evaluation for tissue engineering applications. *J Mater Sci Mater Med* **2010,** *21* (11), 2937-45.

85. Tripathi, A.; Kathuria, N.; Kumar, A., Elastic and macroporous agarose-gelatin cryogels with isotropic and anisotropic porosity for tissue engineering. *J Biomed Mater Res A* **2009,** *90* (3), 680-94.

86. Mishra, R.; Goel, S. K.; Gupta, K. C.; Kumar, A., Biocomposite cryogels as tissue-engineered biomaterials for regeneration of critical-sized cranial bone defects. *Tissue Eng Part A* **2014,** *20* (3-4), 751-62.

87. Plieva, F. M.; Ekström, P.; Galaev, I. Y.; Mattiasson, B. J. S. M., Monolithic cryogels with open porous structure and unique double-continuous macroporous networks. *Soft Matter* **2008,** *4* (12), 2418-2428.

88. Zhao, Q.; Sun, J. Z.; Wu, X. F.; Lin, Y. T., Macroporous double-network cryogels: formation mechanism, enhanced mechanical strength and temperature/pH dual sensitivity. *Soft Matter* **2011,** *7* (9), 4284-4293.

89. Sedlacik, T.; Nonoyama, T.; Guo, H. L.; Kiyama, R.; Nakajima, T.; Takeda, Y.; Kurokawa, T.; Gong, J. P., Preparation of Tough Double- and Triple-Network Supermacroporous Hydrogels through Repeated Cryogelation. *Chem Mater* **2020,** *32* (19), 8576-8586.

90. Yetiskin, B.; Akinci, C.; Okay, O., Cryogelation within cryogels: Silk fibroin scaffolds with single-, double- and triple-network structures. *Polymer* **2017,** *128*, 47-56.

91. Shi, J.; Zhang, H.; Wang, Q.; Duan, Z.; Xu, L.; Guo, F.; Xie, Y.; Chen, Z. J. C. E. J., Biomimetic rigid cryogels with aligned micro-sized tubular structures prepared by conventional redox-induced cryopolymerization in a freezer. *Chem. Eng. J.* **2022,** *427*, 131903.

92. Shariatzadeh, F. J.; Solouk, A.; Khoulenjani, S. B.; Bonakdar, S.; Mirzadeh, H., Injectable and reversible preformed cryogels based on chemically crosslinked gelatin methacrylate (GelMA) and physically crosslinked hyaluronic acid (HA) for soft tissue engineering. *Colloid Surface B* **2021,** *203*.

93. Englund, M.; Roos, E. M.; Lohmander, L. J. A.; Rheumatology, R. O. J. o. t. A. C. o., Impact of type of meniscal tear on radiographic and symptomatic knee osteoarthritis: a sixteen-year followup of meniscectomy with matched controls. **2003,** *48* (8), 2178-2187.

94. Ivanov, R. V.; Lozinsky, V. I.; Noh, S. K.; Han, S. S.; Lyoo, W. S., Preparation and characterization of polyacrylamide cryogels produced from a high-molecular-weight precursor. I. influence of the reaction temperature and concentration of the crosslinking agent. *Journal of Applied Polymer Science* **2007,** *106* (3), 1470-1475.

95. Wex, H.; DeMott, P.; Tobo, Y.; Hartmann, S.; Rösch, M.; Clauss, T.; Tomsche, L.; Niedermeier, D.; Stratmann, F. J. A. C.; Physics, Kaolinite particles as ice nuclei: learning from the use of different kaolinite samples and different coatings. *Atmospheric Chem. Phys.* **2014,** *14* (11), 5529-5546.

96. Weng, L.; Beauchesne, P. R. J. C., Dimethyl sulfoxide-free cryopreservation for cell therapy: A review. *Cryobiology* **2020,** *94*, 9-17.

97. Sakai, T.; Akagi, Y.; Matsunaga, T.; Kurakazu, M.; Chung, U. I.; Shibayama, M., Highly Elastic and Deformable Hydrogel Formed from Tetra-arm Polymers. *Macromol Rapid Commun* **2010,** *31* (22), 1954-9.

98. Wang, H.-Y.; Inada, T.; Funakoshi, K.; Lu, S.-S. J. C., Inhibition of nucleation and growth of ice by poly (vinyl alcohol) in vitrification solution. *Cryobiology* **2009,** *59* (1), 83-89.

99. Wu, J.; Zhao, Q.; Sun, J.; Zhou, Q. J. S. M., Preparation of poly (ethylene glycol) aligned porous cryogels using a unidirectional freezing technique. *Soft Matter* **2012,** *8* (13), 3620-3626.

100. Dispinar, T.; Van Camp, W.; De Cock, L. J.; De Geest, B. G.; Du Prez, F. E., Redox-responsive degradable PEG cryogels as potential cell scaffolds in tissue engineering. *Macromol Biosci* **2012,** *12* (3), 383-94.

101. Wang, J.; Yang, H., Superelastic and pH-Responsive Degradable Dendrimer Cryogels Prepared by Cryo-aza-Michael Addition Reaction. *Sci Rep* **2018,** *8* (1), 7155.

102. Liu, S.; Cao, H.; Guo, R.; Li, H.; Lu, C.; Yang, G.; Nie, J.; Wang, F.; Dong, N.; Shi, J. J. P. D.; Stability, Effects of the proportion of two different cross-linkers on the material and biological properties of enzymatically degradable PEG hydrogels. **2020,** *172*, 109067.

103. Nandiyanto, A. B. D.; Oktiani, R.; Ragadhita, R. J. I. J. o. S.; Technology, How to read and interpret FTIR spectroscope of organic material. *Indones. J. Sci. Technol.* **2019,** *4* (1), 97-118.

104. Lohmander, L. S.; Englund, P. M.; Dahl, L. L.; Roos, E. M. J. T. A. j. o. s. m., The long-term consequence of anterior cruciate ligament and meniscus injuries: osteoarthritis. *Solar Array Gain Augmentation* **2007,** *35* (10), 1756-1769.

105. Christiansen, B. A.; Guilak, F.; Lockwood, K. A.; Olson, S. A.; Pitsillides, A. A.; Sandell, L. J.; Silva, M. J.; van der Meulen, M. C.; Haudenschild, D. R. J. O.; cartilage, Non-invasive mouse models of post-traumatic osteoarthritis. *Osteoarthritis and Cartilage* **2015,** *23* (10), 1627-1638.

106. Adebayo, O. O.; Ko, F. C.; Wan, P. T.; Goldring, S. R.; Goldring, M. B.; Wright, T. M.; van der Meulen, M. C. J. O.; cartilage, Role of subchondral bone properties and changes in development of load-induced osteoarthritis in mice. *Osteoarthritis and Cartilage* **2017,** *25* (12), 2108-2118.

107. Hsia, A. W.; Anderson, M. J.; Heffner, M. A.; Lagmay, E. P.; Zavodovskaya, R.; Christiansen, B. A. J. J. o. O. R., Osteophyte formation after ACL rupture in mice is associated with joint restabilization and loss of range of motion. *Wiley Online Library* **2017,** *35* (3), 466-473.

108. Rai, M. F.; Quirk, J. D.; Holguin, N.; Schmidt, E. J.; Chinzei, N.; Silva, M. J.; Sandell, L. J. J. S. r., Post-traumatic osteoarthritis in mice following mechanical injury to the synovial joint. *scientific reports* **2017,** *7* (1), 1-13.

109. Yan, H.; Pan, H.; Holguin, N.; Rai, M. F.; Akk, A.; Springer, L. E.; Wickline, S. A.; Sandell, L. J.; Pham, C. T. J. P. o. t. N. A. o. S., Suppression of NF-κB activity via nanoparticle-based siRNA delivery alters early cartilage responses to injury. *PNAS* **2016,** *113* (41), E6199-E6208.

110. B Marcu, K.; Otero, M.; Olivotto, E.; Maria Borzi, R.; B Goldring, M. J. C. d. t., NF-κB signaling: multiple angles to target OA. *Current Drug Targets* **2010,** *11* (5), 599-613.

111. Lee, K. M.; Kang, B. S.; Lee, H. L.; Son, S. J.; Hwang, S. H.; Kim, D. S.; Park, J. S.; Cho, H. J. J. E. J. o. N., Spinal NF-kB activation induces COX-2 upregulation and contributes to inflammatory pain hypersensitivity. **2004,** *19* (12), 3375-3381.

112. De Souza, R. L.; Matsuura, M.; Eckstein, F.; Rawlinson, S. C.; Lanyon, L. E.; Pitsillides, A. A. J. B., Non-invasive axial loading of mouse tibiae increases cortical bone formation and modifies trabecular organization: a new model to study cortical and cancellous compartments in a single loaded element. *Bone* **2005,** *37* (6), 810-818.

113. Berke, I. M.; Jain, E.; Yavuz, B.; McGrath, T.; Chen, L.; Silva, M. J.; Mbalaviele, G.; Guilak, F.; Kaplan, D. L.; Setton, L. A., NF-kappaB-mediated effects on behavior and cartilage pathology in a non-invasive loading model of post-traumatic osteoarthritis. *Osteoarthritis Cartilage* **2021,** *29* (2), 248-256.

Resume

Personal information

I'm a master student in Prof. Era Jain's lab at the Biomedical and Chemical Engineering Department, Syracuse University (Syracuse, USA), in which I focused on researching double network cryogels to solve the cartilage defects.

I received my bachelor's degree in chemistry and Materials Science at Northwest University (Xi'an China) where I joined several projects related to functional materials and biomaterials.

I have worked in several research projects through functional materials, inorganic and organic chemistry, and biological science. Besides, I am diligent in study and have a strong ability in learning.

Besides of research, I am also skilled in management. With strong planning and organizing ability, I served as the minister of the Art department of the Student Union during my undergraduate years and organized several large-scale activities such as campus singer contests and evening parties.

Once I have a goal, I will never give it up.

Education

Syracuse University, Syracuse, NY, US   **2019-2021**

- Master of Science in Chemical Engineering
- Research focus: Double network cryogels for cartilage tissue Engineering

Northwest University, Xi'an, Shanxi Province, China   **2014-2018**

- B.S. in Material Chemistry
- Thesis: A Research on the Synthesis, Mechanism and Magnetism of the Modular Unit Compound Based on the $Ru_2(CO_3)_4^{2-}$ Unit and Constructed by Cd^{2+}

Research Experience

Syracuse University, Syracuse, NY, US   **2019-2021**

Graduate researcher in Prof. Era Jain's lab in the Biomedical and Chemical Department

- Double network cryogels were prepared by using alginate and PEG Acrylate and get the interconnect mocroporous structure double network Cryogels.

- Do the different kind of characteristic of double network Cryogels and combine chondrocyte cells with double network Cryogels. Based on the success of cell experiments, it can be used clinically and improve cartilage defects in animals model.

Northwest University, Xi'an, Shanxi Province, China

Undergraduate researcher in Prof. Bin Liu's lab in the college of Chemistry and Materials Science, Material Chemistry   **2016-2018**

- A Research on the Synthesis, Mechanism and Magnetism of the Modular Unit Compound Based on the $Ru_2(CO_3)_4{}^{2-}$ Unit and Constructed by Cd^{2+}

- Towards a new type of heterometallic system based on a paddlewheel Ru_2 dimer: first results derived from the use of a high spin diruthenium (III, III) building block

Undergraduate researcher in Prof. Pengxiang Jia's lab in the college of Chemistry and Materials Science, Material Chemistry   **2014-2016**

- A universal, simple, and efficient surface modification method

  - *surface modification methods suitable for different materials were developed*

  - *Surface modification through polymerization*

- Synthesis of bio-compatible magnetic nanoparticles

Publication

1. Towards a new type of heterometallic system based on a paddle-wheel Ru_2 dimer: first results derived from the use of a high spin diruthenium(iii,iii) building block.

   Bing-Bing Yang, Li-Na Feng, Xiao-Meng Fan, **Kai-Xiang Zhang**, Jian-Hui Yang and

Bin Liu. Inorganic Chemistry Frontiers. April 28,2017

Conference

1. "Double network cryogels scaffold for repair of focal cartilage defect", Stevenson Biomaterials Poster Session, Syracuse university 2021

2. 7th National Structural Chemistry Academic Conference, Guangzhou, China. 2016

3. 15th National Annual Meeting of Applied Chemistry, Tianjin, China, 2017

Relevant Professional Course

Organic chemistry, Inorganic chemistry, High polymer chemistry, Biochemistry, Physical chemistry, Analytical chemistry, Spectral principles, Drug delivery, Fluid mechanics, Thermodynamics, Dynamics, Material chemistry, Chemical structure, Chemical engineering principles

Certificates

1. 2017 XIBEI University Chemistry-Biology Experience at the Ohio State University, Ohio State University, 2017

2. Data Science in Biomedical and Chemical Engineering, Syracuse University, 2020

Honor

University-level scholarship, Northwestern University, China, 2016-2017